R. & M. No. 3382

MINISTRY OF AVIATION

AERONAUTICAL RESEARCH COUNCIL
REPORTS AND MEMORANDA

An Experiment on Aerodynamic Nozzles at $M = 2$

By J. Reid

LONDON: HER MAJESTY'S STATIONERY OFFICE
1964
PRICE 15*s*. 0*d*. NET

An Experiment on Aerodynamic Nozzles at $M = 2$

By J. Reid

Communicated by the Deputy Controller Aircraft (Research and Development), Ministry of Aviation

*Reports and Memoranda No. 3382**

November, 1962

Summary.

In an aerodynamic nozzle a convergent primary nozzle is housed within an afterbody which is surrounded by a shroud. Part of the external flow is captured thereby and compressed by the under-expanded primary jet. At the design point this system is not as efficient as a convergent-divergent nozzle but its off-design performance should be better.

In the experiment axi-symmetric models were used. The shrouds were cylindrical externally and either cylindrical or convergent-divergent internally. With each model the thrust and afterbody pressure distributions were measured at jet pressure ratios up to 20 with a free-stream Mach number of 2·0. Component drags were estimated indirectly from these measurements. For comparison, the thrust of unshrouded convergent and convergent-divergent nozzles was measured under the same conditions.

With the cylindrical shrouds the effects of shroud length, shroud diameter and boundary-layer thickness were investigated. The greatest thrust developed by these models was about 5% less than that of the equivalent convergent-divergent nozzle. With the convergent-divergent shrouds the main variable studied was the ratio shroud throat area/shroud exit area. The thrust of the best model was some 9% less than that of the convergent-divergent reference nozzle.

In the case of one cylindrical shroud the internal flow was studied in detail by surface pressure measurements and radial traverses.

LIST OF CONTENTS

* Replaces R.A.E. Report No. Aero. 2672—A.R.C. 24 845.

LIST OF CONTENTS—*continued*

Section

LIST OF ILLUSTRATIONS

Figure

---

1. *Introduction.*

With long-range supersonic aircraft a slight increase in specific fuel consumption at the cruising speed seriously decreases the payload. One essential requirement of the propelling nozzle in such aircraft is, therefore, a high efficiency at the design cruising speed. A second requirement is imposed by the need to accelerate the aircraft through the transonic speed range. This phase is of short duration so that the specific fuel consumption is relatively unimportant. The difficulty is to obtain thrust in excess of the high transonic drag with the comparatively low jet-pipe pressure available at transonic speeds. To achieve this, reheat may be needed, but the nozzle efficiency is also an important factor.

Now the jet pressure ratio (jet-pipe total pressure/free-stream static pressure) available at a given flight speed depends on the type of engine considered. For present purposes, however, we may take representative values of 5 at $M = 1$ and 15 at $M = 2$. On this basis a convergent nozzle develops about 97% of the ideal thrust at $M = 1$ and about 90% of the ideal thrust at $M = 2$. At both speeds the loss in thrust is due to under-expansion. The performance at $M = 1$ might just suffice, but the loss in thrust at the cruising speed ($M = 2$) could not be tolerated.

Consider next a convergent-divergent nozzle of fixed geometry which expands the jet isentropically down to free-stream static pressure at the cruising speed (Fig. 1a). Theoretically this type of nozzle gives the maximum possible thrust under these conditions and in practice the actual thrust lies within 2 or 3% of this ideal. However, at jet pressure ratios much below the design value the performance deteriorates because of over-expansion, accompanied by separation of the flow within

the nozzle (Fig. 1b). Effectively, the nozzle surface downstream of the separation point acts as a base and the resultant thrust is seriously decreased by the high base drag.

Various methods of achieving a high nozzle efficiency over a range of jet pressure ratio have been proposed. The first, and most obvious of these, is to use a convergent-divergent nozzle with movable side walls, so that the expansion ratio can be varied to suit the jet pressure ratio. This is a practical solution, at least for a 'two-dimensional' nozzle, but it implies a weight penalty and an increase in mechanical complexity. An alternative design is the plug nozzle in which the supersonic expansion is constrained partly by the surface of the plug and partly by conditions along the free boundary between the jet and the external stream. In yet a third possibility part of the free stream is constrained by a shroud and used to control the supersonic expansion of the jet from a convergent nozzle. Systems of this type, which we shall call 'aerodynamic' nozzles*, form the subject of the present paper.

2. *The Aerodynamic Nozzle.*

A representative example of an aerodynamic nozzle is shown in Fig. 2a. Its principle of operation is best explained by considering the effect of jet pressure ratio on the flow within the shroud.

When the jet pressure ratio is small, the primary flow will be subsonic and the secondary flow supersonic throughout. Under these conditions the pressure at all points on the afterbody will be less than the static pressure in the free stream so that the afterbody is subject to a drag. As the jet pressure ratio is steadily increased the primary flow will first choke in the throat of the primary nozzle and will then expand supersonically downstream of this throat. When this occurs the diverging primary flow restricts the secondary flow and an oblique shock wave traversing the secondary stream is formed at the trailing edge of the afterbody. Further increase in jet pressure ratio causes this shock to strengthen and to bifurcate, and both the shock system and its attendant separation bubble move upstream. When the shock system has reached the shroud intake lip (as shown in Fig. 2a) the secondary flow over the afterbody is largely subsonic and the pressure on the afterbody is considerably greater than the free-stream static pressure. The afterbody is therefore subject to a thrust. Moreover, since the axial force on a thin cylindrical shroud is relatively small, and the forces inside the choked primary nozzle are independent of the external flow, the thrust minus the drag of the configuration will be greater with the shroud than without.

It is worth noting that, in some respects, the aerodynamic nozzle sketched in Fig. 2a closely resembles the side intake with control flap sketched in Fig. 2b. Increasing the jet pressure ratio in the former example has much the same effect as decreasing the exit area in the latter example. In both cases a shock system moves progressively upstream so that a thrust is exerted on the afterbody or the diffuser respectively. There is, however, one essential difference between the two models. In Fig. 2b the flow is restricted by a solid surface (the exit flap) and the thrust force on the diffuser is offset by the drag force on the flap. On the other hand, in Fig. 2a the secondary flow is restricted by the diverging free boundary between the primary and secondary streams, and the thrust force on the afterbody is therefore generated without incurring drag. This is the basic principle of the aerodynamic nozzle. To look at the problem from a slightly different viewpoint, the thrust force on the divergent part of a conventional convergent-divergent nozzle is, in the case of the aerodynamic nozzle, transferred upstream to the afterbody *via* the subsonic secondary flow.

* These are often referred to as 'ejector' nozzles. The name suggested is considered preferable.

It is convenient to distinguish three types of secondary flow, as shown in Fig. 3. When the shock system lies within the shroud the secondary intake is said to be super-critical (Fig. 3a). Conversely, sub-critical operation implies that the shock system is located upstream of the shroud lip (Fig. 3c). When the shock is on the shroud lip (Fig. 3b) both the intake and the corresponding jet pressure ratio are said to be critical. The secondary mass flow is constant throughout the super-critical regime, but in the sub-critical regime the capture area is reduced, the intake 'spills', and the secondary mass flow decreases.

It should be emphasised that the nozzles and flow patterns sketched in Figs. 2a and 3 are merely representative. The essential features are, firstly, a convergent nozzle whose throat area is less than that of the centrebody; and secondly, the provision of some form of shroud. The shroud, however, need not necessarily be cylindrical, nor need the afterbody be conical. These points will be discussed in more detail later. Further, although the nozzle sketched is axi-symmetric, the design is equally applicable to a configuration which is rectangular in section.

In Figs. 2a and 3 the secondary intake is situated at the shoulder of the afterbody so that the secondary flow is derived from the free stream and the boundary layer over the centrebody. In general, however, the secondary flow may be supplied by any convenient source with the requisite stagnation pressure. For example, an attractive engine installation is achieved if boundary-layer bleed from the main engine intake provides the secondary air for an aerodynamic propulsion nozzle. At the same time, whichever configuration is adopted, it is clear that the efficiency of the aerodynamic nozzle will depend in large measure on the pressure recovery in the secondary intake, and this in turn will depend on the ratio of boundary-layer thickness to intake height. The bifurcated normal shock shown in Figs. 2a and 3 is, in fact, but one member of a family of shock systems ranging from an oblique shock when the boundary layer is relatively thick to a simple normal shock in the limiting case when there is no boundary layer.

Finally we note that mixing processes are not fundamental to the operation of an aerodynamic nozzle. Comparatively short shrouds, a few primary-nozzle diameters in length, should therefore be effective. Previous experience[1] indicates that very little mixing occurs over this range of shroud length.

3. *The Experimental Programme.*

Acoustic measurements have shown that a short shroud is a relatively poor attenuator of noise. The practical value of the aerodynamic nozzle may therefore be assessed in terms of thrust. On this basis, information is needed on the thrust developed at the design cruising speed and also at lower flight speeds, particularly in the transonic range. However, to limit the amount of experimental work, it was decided to study the performance at the design point first and, if the results looked promising, to follow this investigation with transonic tests on the more worthwhile designs at a later date. This report is therefore concerned solely with the characteristics of aerodynamic nozzles at an assumed cruising Mach number of 2·0.

In the past, aerodynamic nozzles have been studied fairly extensively[2 to 8], but in this earlier work the secondary stream was supplied through a pipe at controlled values of the stagnation pressure. Capture of the boundary layer and free stream by the secondary intake and compression within the secondary diffuser were not investigated. The present experiment differs in that the complete aerodynamic nozzle including the secondary intake and diffuser are simulated. Similar work on a two-dimensional aerodynamic nozzle has recently been completed at R.A.E. by Jessop[9].

The type of configuration tested is shown in Fig. 4†. It will be seen that the primary nozzle is axi-symmetric and convergent, and the afterbody is conical with only a small base annulus. The shroud is cylindrical externally, but internally it may be either cylindrical or convergent-divergent. In the latter case the throat of the shroud lies one primary-nozzle diameter downstream of the primary-nozzle exit plane. In all cases the shroud entry lip is level with the shoulder of the afterbody.

The properties of the configurations shown in Fig. 4 are largely determined by eight independent variables. These are:

$$M_\infty, \frac{{}_tp_j}{p_\infty}, \beta, \frac{a_1}{a_0}, \frac{a_2}{a_0}, \frac{a_4}{a_3}, \frac{l_{13}}{d_1} \text{ and } \frac{\delta^*}{h_2}$$

{note that (i) $a_4/a_3 = 1$ for the cylindrical shrouds

and (ii) $M_\infty = 2{\cdot}0$ throughout the experiment}.

For the models with cylindrical shrouds, the effect of a_2/a_0, l_{13}/d_1 and δ^*/h_2 on the nett thrust was studied systematically over a range of jet pressure ratio (${}_tp_j/p_\infty$). In this series of tests β and a_1/a_0, were maintained constant. The nett thrust of each model was compared with the nett thrust of two unshrouded reference nozzles, each of which had the same afterbody angle (β) and the same ratio of throat area/centrebody area (a_1/a_0) as the shrouded nozzle. These reference models were:

(1) A simple convergent nozzle.

(2) A conical convergent-divergent nozzle designed for a jet pressure ratio of 10.

For the models with convergent-divergent shrouds β, a_1/a_0, a_2/a_0, l_{13}/d_1 and δ^*/h_2 were maintained constant and the effect of a_4/a_3 was investigated over a range of ${}_tp_j/p_\infty$. In this case also, an unshrouded convergent nozzle and an unshrouded convergent-divergent nozzle with a design pressure ratio of 10 served as reference standards.

To supplement the thrust data a fairly detailed study was made of the flow within a shroud at several values of jet pressure ratio. For this purpose one model with a cylindrical shroud was chosen, and the static-pressure distribution measured along the afterbody and the internal surface of the shroud. In addition, velocity profiles were measured in the primary-nozzle exit plane and the shroud exit plane, and schlieren photographs were taken of the flow at the shroud intake and exit.

These data throw some light on the mechanism of pressure recovery in the secondary flow and also on the nature of the interaction between the primary and secondary streams. They also furnish direct evidence on conditions in the shroud exit plane. This is a matter of some interest since, in the theoretical approach to the problem, some of the necessary boundary conditions are determined by the flow parameters at the shroud exit.

4. *Theoretical Work.*

Of the various methods suggested for calculating the thrust of an aerodynamic nozzle, the theories of Kochendorfer[2] and Pearson[8] have been selected for special comment. Each of these investigators considers the simplest model in which a convergent axi-symmetric primary nozzle discharges into

† Fig. 4, together with the List of Symbols, shows also the notation used in the report, excepting the definitions of thrust and drag coefficients. These latter, and the relations between them, are given in the Appendix.

a short cylindrical shroud. This is the configuration shown in Fig. 4 (with $a_4/a_3 = 1$). Moreover, the following assumptions are common to both theories.

(i) At planes (1) and (3) [Fig. 4] the flow in both the primary and secondary streams is parallel to the axis and uniform.

(ii) In plane (3) [Fig. 4] the static pressure of the secondary stream is equal to that of the primary stream and greater than atmospheric pressure.

(iii) In plane (1) [Fig. 4] the Mach number of the primary stream is unity.

(iv) No mixing occurs between the primary and secondary streams within the shroud.

(v) No skin friction at the shroud wall.

The analytical procedure also is essentially the same. The flow between planes (1) and (3) [Fig. 4] is considered and two equations obtained by applying the continuity relation to the primary and secondary flows. A third equation follows from the momentum theorem applied to the combined flows. It is found, however, that these three equations are insufficient to solve the problem as specified, the flow being indeterminate. To obtain a unique solution for given values of the stagnation pressure ratio and flow area ratio at entry, two more equations are required and hence two more assumptions must be made. It is in formulating these two extra assumptions that the two authors differ.

Kochendorfer postulates:

(vi) That the primary flow is isentropic.

(vii) That the Mach number of the secondary stream is unity at the shroud exit.

On this basis he calculates the mass-flow ratio and thrust over a range of operating conditions and obtains quite fair agreement with his experimental results.

Pearson, on the other hand, originally assumed:

(viii) That the secondary flow is isentropic.

(ix) That the Mach number of the secondary stream is unity at the shroud exit.
[Note that assumptions (vii) and (ix) are identical.]

On this basis, experiment and theory disagreed. Faced with this fact, Pearson retained (viii) but replaced (ix) by the following hypothesis.

(x) That for given values of the stagnation pressure ratio and flow area ratio at entry, the secondary mass flow is the maximum possible consistent with the equations of continuity and momentum.

With these assumptions {(viii) and (x)}, satisfactory agreement between theory and experiment was achieved.

Some comment on the status of assumptions (vi), (vii), (viii) and (x) is desirable. In the first place it is clear that (vi) is not strictly true because the primary jet is under-expanded and is therefore traversed by shock waves. Assumption (vii) however, would appear to be justified since the theory assumes that the shroud is cylindrical and [by (ii)] the uniform static exit pressure is greater than atmospheric. Nevertheless, as shown below, it is possible to argue otherwise. Assumption (viii) also is reasonable, because the secondary flow is subsonic and [by (iv)] there is no mixing between the two streams. On the other hand (x) which, at first sight, does not appear to be based on any known physical principle, has led to controversy. It implies, as Pearson himself has shown, that a

relation exists between the Mach numbers of the primary and secondary streams and their area ratio at the shroud exit. Moreover, this equation is such that if the primary stream is supersonic, then the secondary stream is subsonic. Since the static pressure in the exit plane is, by hypothesis, greater than atmospheric, this conclusion is difficult to accept. In justification, Pearson argues that the secondary flow is effectively bounded internally by a flexible wall (the primary flow) and in the circumstances the velocity of sound in the secondary flow is not given by the usual formula. He develops this argument mathematically but it would seem that his analysis has not met with unqualified acceptance.

The correct boundary values of the problem are therefore not known with certainty and direct experimental evidence is needed on the flow parameters in the shroud exit plane. Some of this evidence was obtained in the present experiment and this will be discussed in Section 8.1.

5. *Description of Wind Tunnel and Models.*

5.1. *The Tunnel.*

The Royal Aircraft Establishment Jet Interference Tunnel shown in Fig. 5 was used for the experiment. This is a continuous-running supersonic tunnel designed specifically to minimise support interference in tests with mixed exhaust flows. To this end the main tunnel nozzle is axi-symmetric ($M = 2$), and the test-model is mounted on the end of a long, double-skinned cylindrical tube (the centrebody) which passes through the throat of the nozzle and its settling chamber into a separate plenum chamber. Pressure leads from the test-model pass between the two skins of the centrebody to a multi-point connector and thence to mercury manometers.

Dry air at 1 atm. abs. stagnation pressure is supplied to the main tunnel nozzle, while the primary nozzle in the test-model is fed, *via* the centrebody, with undried air at a maximum stagnation pressure of 2 atm. abs. The stagnation temperature of both supplies is about 20°C. A simple hydraulic balance measures the thrust and drag forces on the model and a schlieren system is available for flow visualisation. A detailed description of the Jet Interference Tunnel has been published elsewhere[10].

5.2. *The Models.*

5.2.1. *Models with cylindrical shrouds.*—The nozzle used in conjunction with cylindrical shrouds is shown in Fig. 6. It is convergent and is housed in a conical afterbody with a semi-vertex angle (β) of 10°. To permit installation of the pressure points the model was made in two concentric parts. Accordingly, it was not possible to eliminate the base entirely, but the base area is relatively small. In meridian section the nozzle profile is formed by a straight tapered approach section joined tangentially to a straight throat section (parallel to the axis) by a circular arc of radius equal to the throat diameter. Ten static-pressure points are installed along one generator of the afterbody, but because of practical difficulties there are no pressure points in the base annulus. The ratio throat area/centrebody area (a_1/a_0) is 0·45 so that the nozzle is designated C.45*.

The cylindrical shrouds were made of 20 s.w.g. brass with the leading edge chamfered internally at 10° to the axis to form a sharp lip at entry. Three thin fins, equally spaced, serve to hold the

* For brevity, the various nozzles are identified by letters (C or C-D) followed by a number. 'C' denotes a convergent nozzle, 'C-D' a convergent-divergent nozzle, and the number is equal to $100 \times a_1/a_0$.

shrouds concentric with the afterbody with the entry lip level with the afterbody shoulder. A sketch of the complete assembly is shown in Fig. 7.

Seven cylindrical shrouds were tested in all, the geometrical details being shown in Table 1. (Note that Nos. 1 and 6 are identical.)

TABLE 1

Cylindrical Shrouds ($a_4/a_3 = 1$)

No.	a_2/a_0	l_{13}/d_1
1	0·69	1·0
2	0·69	2·0
3	0·69	3·0
4	0·00	1·0
5	0·37	1·0
6	0·69	1·0
7	1·04	1·0
8	1·42	1·0

It will be seen that these form two groups. In the first group l_{13}/d_1 is varied with a_2/a_0 constant, whereas in the second group the converse applies.

Three versions of shroud No. 1 were made. The first, which was not instrumented, was used for thrust measurement. A row of static-pressure points was installed along one generator of the second in order to measure the distribution of static pressure along the internal wall. These static points were in line with the corresponding set along the afterbody. The third version, which was equipped with a pitot traverse gear, served for the measurement of velocity profiles at two axial stations; namely, the shroud exit plane and the primary-nozzle exit plane. None of the other cylindrical shrouds was instrumented.

5.2.2. *Models with convergent-divergent shrouds.*—Fig. 8 shows the nozzle used with the convergent-divergent shrouds. This model is similar to that described above in that the nozzle is convergent, the base annulus small and the afterbody conical with a semi-vertex angle of 10°. The nozzle profile and the distribution of pressure points are also similar. However, to maintain the critical jet pressure ratio within the required range, the ratio throat area/centrebody area (a_1/a_0) is reduced to 0·25. The nozzle is therefore designated C.25.

Fig. 9 gives details of the convergent-divergent shrouds. These were made in two parts; namely, a cylindrical sheath and a detachable convergent-divergent insert called the 'choke'. In meridian section the choke profile is formed by two straight lines inclined to the axis, joined tangentially by a circular arc. The throat of the choke is situated one primary-nozzle diameter downstream of the primary-nozzle exit plane. The complete shroud is secured to the afterbody by three fins, with the sharp leading edge of the shroud level with the afterbody shoulder.

A series of six convergent-divergent shrouds was tested. In this series a_2/a_0 and l_{13}/d_1 were maintained constant while a_4/a_3 was varied. The geometrical details are given in Table 2.

TABLE 2

Convergent-Divergent Shrouds
($a_2/a_0 = 0{\cdot}73$, $l_{13}/d_1 = 4{\cdot}0$)

No.	a_4/a_3
9	0·58
10	0·64
11	0·71
12	0·77
13	0·85
14	1·00

5.2.3. *Reference models.*—The nett thrust developed by the nozzle C.45 with cylindrical shrouds is compared with the nett thrust of two reference models. One of these is the unshrouded C.45 nozzle. The other is the nozzle C-D.45 sketched in Fig. 10a. This is a conical convergent-divergent nozzle with a design pressure ratio of 10. The afterbody is cylindrical, the nozzle divergence angle is 5° and the ratio throat area/centrebody area equals 0·45.

Similarly the nett thrust of C.25 with the convergent-divergent shrouds is compared with the nett thrust of the unshrouded C.25 nozzle and also with the nett thrust of the nozzle C-D.25 shown in Fig. 10b. This is a conical convergent-divergent nozzle installed in a conical afterbody. The nozzle is designed for a pressure ratio of 10; the nozzle divergence angle and afterbody angle are 5° and 10° respectively, and the ratio throat area/centrebody area is equal to 0·25.

6. *Experimental Procedure.*

6.1. *The Centrebody Boundary Layer.*

In a previous experiment[10] it was shown that the boundary layer on the centrebody is turbulent, and the thickness was measured at several axial stations within the test section. In the present tests these data were used to determine the boundary-layer parameters at the afterbody shoulder, and hence the value of δ^*/h_2. This quantity was varied either by changing the shroud diameter or by axial movement of the model.

6.2. *Shroud Pressures and Velocity Profiles.*

The static-pressure distribution along the internal surface of the shroud was measured in the case of one model only; namely, nozzle C.45 combined with shroud No. 1 (Table 1). These data were obtained at four values of the jet pressure ratio ($_1p_j/p_\infty = 6$, 12, 16 and 18) with $\delta^*/h_2 = 0{\cdot}12$. With the same model, and under the same conditions, pitot- and static-pressure traverses were made across one radius at two axial stations. The radius lay in the meridian plane through the shroud pressure points. The axial stations selected were the shroud exit plane and the primary-nozzle exit plane.

6.3. *Afterbody Pressures.*

The surface pressure distribution along the afterbody was measured in the case of all models with shrouds. These comprise:

(1) Nozzle C.45 and cylindrical shrouds Nos. 1 to 8 (Table 1).

(2) Nozzle C.25 and convergent-divergent shrouds Nos. 9 to 14 (Table 2).

With each model these data were obtained at a number of values of jet pressure ratio between 2 and 20. δ^*/h_2 lay in the range of 0·03 to 0·12.

6.4. *Thrust Measurements.*

Balance measurements of the nett thrust were taken with all shrouded models and also with the four unshrouded reference nozzles (C.25, C.45, C-D.25 and C-D.45). The thrust was measured at a number of values of ${}_tp_j/p_\infty$ in the range 2 to 20. δ^*/h_2 ranged between 0·03 and 0·12.

6.5. *Schlieren Photographs.*

In the case of one model (nozzle C.45 and shroud No. 1) a set of schlieren photographs was taken showing the effect of jet pressure ratio on the flow at the shroud entry and exit. ${}_tp_j/p_\infty$ ranged from 6 to 20 and δ^*/h_2 was equal to 0·12.

7. *Analysis of Thrust Data.*

(Note. Thrust and drag coefficients are defined in the Appendix.)

To determine the contribution made by the various components to the nett thrust, the data were analysed as follows:

(1) The balance readings, corrected for skin-friction drag on the centrebody and out-of-balance pressures in the different tunnel chambers give $(C_T)_J - [(C_D)_A + (C_D)_B + (C_D)_S]$.

(2) A run was made with no external flow and the shroud removed. Under these conditions $(C_D)_A = (C_D)_B = (C_D)_S = 0$ so that the balance readings give $(C_T)_J$. Note that for a choked convergent nozzle $(C_T)_J$ depends only on a_1/a_0 and ${}_tp_j/p_\infty$ and is independent of the geometry of afterbody, base and shroud.

(3) $(C_D)_A$ was calculated by numerical integration of the measured afterbody pressure distribution. This method assumes firstly that the pressure distribution is axi-symmetric and secondly that the skin-friction drag is negligible. A direct experimental check of the first assumption was not made but schlieren photographs (Fig. 12) indicate a fair degree of symmetry except during sub-critical operation. The second assumption is probably justified since the shear layer on the afterbody is either thick (Fig. 13) or separated (Figs. 14 to 16).

(4) $(C_D)_B$ was calculated assuming the base pressure to be equal to the static pressure on the afterbody in the base plane. This is a reasonable assumption because the shear layer at the trailing edge of the afterbody is thick compared with the width of the base annulus.

(5) $(C_D)_S$ was obtained by subtraction.

Using the unshrouded C.25 nozzle a partial check was made of possible sources of error in steps (3) and (4) above. In this check $(C_T)_J - [(C_D)_A + (C_D)_B]$ was first determined from balance

readings with external flow. Similar measurements in a static atmosphere gave $(C_T)_J$ and hence $(C_D)_A + (C_D)_B$ by difference. These values of $(C_D)_A + (C_D)_B$ were compared with the corresponding values calculated from the measured afterbody pressure distribution as outlined above. The difference between the two sets of readings was of the same order as the experimental scatter and was not systematic.

In presenting the thrust data the overall performance of each aerodynamic nozzle is assessed in terms of the nett thrust coefficient (C_T') [*see*, e.g. Fig. 21]. Also shown are the component drag coefficients $(C_D)_A + (C_D)_B$ and $(C_D)_S$ [*see*, e.g. Fig. 20]. It is to be noted that the accuracy of the values quoted for C_T' should be adequate because this quantity depends only on the difference of two balance readings. On the other hand the component drag coefficients, which are derived indirectly, are probably less accurate.

8. *Discussion of Results. Tests with Cylindrical Shrouds.*

8.1. *The Flow within the Shroud.*

In this section we will consider, in some detail, the type of flow produced by interaction between the primary and secondary streams inside the shroud. Points of particular interest are the mechanism of compression in the secondary stream, the degree of mixing between the two streams, and the form of the velocity profile at the shroud outlet. Experimental evidence on these points was obtained using the C.45 nozzle and a cylindrical shroud with $a_2/a_0 = 0{\cdot}69$ and $l_{13}/d_1 = 1{\cdot}0$.

The effect of the primary stream on the secondary stream is clearly shown by the afterbody pressure distributions plotted in Fig. 11 and the schlieren photographs of Fig. 12. Referring to Fig. 11 we note that the afterbody pressure distribution is not affected by jet pressure ratio provided that ${}_tp_j/p_\infty \leqslant 8$. Over this range a weak shock from the shroud entry lip gives rise to a hump in the distribution at about $x/l_{12} = 0{\cdot}2$ and this compression, together with the relatively thick boundary layer, practically suppresses the Prandtl-Meyer expansion at the afterbody shoulder.

As ${}_tp_j/p_\infty$ is increased the primary stream expands outside the choked primary nozzle and restricts the secondary stream. As a result the secondary flow separates from the surface of the afterbody and a shock forms at the point of separation. Judging by the shape of the pressure distributions, the flow does not reattach to the afterbody surface. With increasing jet pressure ratio the separation point moves upstream, reaching the afterbody shoulder when ${}_tp_j/p_\infty = 15$ and pausing there until ${}_tp_j/p_\infty = 16$. Up to this point no disturbance at the shroud intake is visible in the schlieren photographs of Fig. 12. At higher jet pressure ratios, however, separation moves forward along the centrebody and when ${}_tp_j/p_\infty = 18$ the relevant photograph in Fig. 12 shows that the shock intersects the shroud entry lip†. This condition corresponds to critical operation. With further increase in ${}_tp_j/p_\infty$ (sub-critical operation) the intake spills and the secondary mass flow decreases but Fig. 11 shows that pressure recovery along the afterbody is increased very little thereby. Moreover, under these conditions, the intake flow tends to become unsteady and asymmetric, a feature common to most intakes in the presence of a boundary layer.

† It is apparent from Fig. 12 that when the secondary intake is critical or sub-critical the flow at entry is not strictly symmetrical. Under these conditions oil-flow patterns showed that the line of separation around the centrebody lay in a plane normal to the axis except for a small region at the top of each photograph. In Fig. 12 the pressure points lie in a plane through the axis perpendicular to the plane of the paper. In comparing Figs. 11 and 12, therefore, the flow pattern at the bottom of each photograph is to be considered.

It is worth noting that if the boundary layer on the centrebody were of zero thickness, compression of the secondary stream would be brought about by a plane normal shock and the resultant pressure recovery would be approximately twice that shown in Fig. 11. It is therefore clear that δ^*/h_2 has a very marked effect on both the mechanism and the magnitude of the pressure recovery in the secondary stream.

A more detailed survey of the flow was made at jet pressure ratios of 6, 12, 16 and 18, and the results are summarised in Figs. 13 to 16 respectively. Each of these figures consists of three parts. At the bottom of each sheet the radial distribution of Mach number at three axial stations is super-imposed on a scale drawing of the model. The axial stations referred to are situated slightly ahead of the afterbody shoulder, in the primary-nozzle exit plane, and in the shroud exit plane, respectively. Above this drawing is a graph of the streamwise variation in static pressure along the surface of the afterbody and the internal surface of the shroud. Finally, at the top, is a scale diagram showing the estimated positions of the more important features of the flow. These flow diagrams were constructed by inference from the Mach number profiles, surface pressure distributions, and schlieren photographs of the external flow (Fig. 12). They are therefore based mainly on indirect evidence and for this reason certain details, such as the exact form of the shock systems and the extent of separated regions, may not be strictly correct. Nevertheless, the diagrams probably give a fair picture of the essentials of the flow pattern.

In Fig. 13 ($_tp_j/p_\infty = 6$) the jet pressure ratio is not high enough to promote separation on the afterbody surface, the secondary stream being compressed by an oblique shock at the trailing edge of the afterbody. The effects of this shock on the shroud pressure and the Mach number profile in the shroud exit plane are clearly seen in Fig. 13 and the shock itself is visible in Fig. 12. Note also that although separation does not occur, the shear layer on the afterbody is relatively thick. Excluding this shear layer and the boundary layer on the internal surface of the shroud, the secondary stream is supersonic throughout and, indeed, its Mach number appears to change very little from the entry to the exit.

At a jet pressure ratio of 12 the picture is slightly different (Fig. 14). The afterbody and shroud pressures show that separation now occurs about halfway along the afterbody, and the Mach number profiles indicate that the separation bubble is still open in the primary-nozzle exit plane. The shroud pressures give evidence that a second shock forms where the separated, but partly supersonic, secondary stream meets the expanding primary stream.

The pressure distributions of Fig. 15 indicate that when $_tp_j/p_\infty = 16$ the separation point has reached the afterbody shoulder. The oblique shock at separation and its reflections give rise to rapid streamwise variations in shroud pressure but these are soon damped out by the separated region adjacent to the afterbody. The form of the Mach number profile in the exit plane of the primary nozzle implies flow reversal within the separation bubble close to the afterbody surface although the measurements were not sufficiently sensitive to provide direct evidence on this point (but see below). A normal shock is probably still present in the supersonic part of the secondary flow in the region where the secondary stream meets the primary stream.

Fig. 16 corresponds to the critical jet pressure ratio ($_tp_j/p_\infty = 18$). Both the afterbody and shroud pressures in this figure, and the schlieren photographs in Fig. 12, provide evidence that the separation shock intersects the shroud entry lip under these conditions. The Mach number profile at the trailing edge of the afterbody testifies to a thick separated region at this station. That this separated region extends over the entire length of the afterbody was confirmed by oil-flow tests.

Small quantities of oil introduced into the primary-nozzle supply pipe formed a ring of liquid around the centrebody just upstream of the afterbody shoulder, thus demonstrating flow reversal and at the same time marking the line of separation of the secondary stream. Downstream of the primary nozzle the secondary flow is largely subsonic.

Certain features of the flow, which are common to all four values of jet pressure ratio, are relevant to the theoretical discussion of Section 4. Referring to Figs. 13 to 16 and the schlieren photographs (Fig. 12) we note, firstly, that the primary flow contains shock waves. This shock system is, of course, a well known characteristic of the flow from an under-expanded convergent nozzle. As a result, both the Mach number, static pressure and total pressure of the primary stream are non-uniform in the shroud exit plane. Assumptions (i), (ii) and (vi) of Section 4 are, therefore, incorrect. The experiment yields little information about assumptions (iv), (v) and (viii) but the traverses in the exit plane of the primary nozzle confirm the truth of assumption (iii). On the other hand, the profiles at the shroud exit indicate that the Mach number in the secondary stream (excluding the boundary layer and mixing region) varies from about $1 \cdot 0$ when ${}_tp_j/p_\infty = 18$ to about $1 \cdot 8$ when ${}_tp_j/p_\infty = 6$. Consequently assumption (vii) [and (ix)] is not generally true although it approximates to the truth at the higher jet pressure ratios. Pearson's special hypothesis (x), which predicts that when the primary stream is supersonic the secondary stream must be subsonic, likewise appears to be incorrect.

To sum up, assumptions (i), (ii) and (vi) of Kochendorfer's theory are at variance with the evidence, while assumption (vii) is only approximately true at the higher jet pressure ratios. Similarly, the experiment is not in agreement with assumptions (i), (ii) and (x) in Pearson's (final) theory. While exact correspondence between theory and experiment is not to be expected, in the present instance the discrepancies are rather large. Unfortunately the experiment does not suggest a simple and consistent set of boundary conditions with which to replace those of Kochendorfer and Pearson.

8.2. *Thrust Data.*

8.2.1. *The effect of ${}_tp_j/p_\infty$ on the thrust.*—So far we have described the changes which take place in the flow as the jet pressure ratio is increased. We have now to examine the effect of these changes on the thrust. These thrust data apply to the model used in the previous experiment; namely, the C.45 nozzle and a cylindrical shroud with $a_2/a_0 = 0 \cdot 69$ and $l_{13}/d_1 = 1 \cdot 0$. The boundary layer is thinner ($\delta^*/h_2 = 0 \cdot 06$ compared with $\delta^*/h_2 = 0 \cdot 12$) but, comparing the afterbody pressure distribution shown in Fig. 17 ($\delta^*/h_2 = 0 \cdot 06$) with the corresponding distribution shown in Fig. 11 ($\delta^*/h_2 = 0 \cdot 12$) it is apparent that this change in boundary-layer thickness has but a slight effect on the flow.

In Fig. 18a the afterbody plus base drag coefficient $[(C_D)_A + (C_D)_B]$ and the shroud drag coefficient $[(C_D)_S]$ are plotted against jet pressure ratio. It will be seen that the gradient of the $(C_D)_A + (C_D)_B$ curve is discontinuous at two points. Comparison with Fig. 17 shows that one of these discontinuities (${}_tp_j/p_\infty = 6 \cdot 8$) occurs when the separation point leaves the trailing edge of the afterbody. The other (${}_tp_j/p_\infty = 19 \cdot 2$) occurs at the critical jet pressure ratio. On the other hand $(C_D)_S$ is relatively insensitive to jet pressure ratio and the gradient of the curve is apparently continuous. At the lower jet pressure ratios the change in $(C_D)_S$ is probably due mainly to a change in base drag, whereas when ${}_tp_j/p_\infty > 17$, forward motion of the separation shock increases the pressure drag at the leading edge of the shroud.

The sum of the component drag coefficients $[(C_D)_X]$ is plotted against ${}_tp_j/p_\infty$ in Fig. 18b. It is important to note that the optimum operating point, corresponding to the minimum value of $(C_D)_X$, occurs at the critical jet pressure ratio.

The relative magnitude of the total component drag $[(C_D)_X]$ and the jet thrust $[(C_T)_J]$ is brought out by the two curves in Fig. 19. At the critical jet pressure ratio, for example, $(C_D)_X$ is only some 5% of $(C_T)_J$. Consequently if the models are compared on the basis of $(C_T)_J - (C_D)_X$ the curves lie close together and are difficult to resolve. In subsequent graphs, therefore, the performance of each model is assessed in terms of the nett thrust coefficient $C_T' = (C_T)_J - (C_T)_J^* - (C_D)_X$. (See Appendix.)

8.2.2. *The effect of l_{13}/d_1 on the thrust.*—Three shrouds of the same diameter ($a_2/a_0 = 0{\cdot}69$) and different lengths ($l_{13}/d_1 = 1$, 2 and 3) were tested in combination with the C.45 nozzle. The component drag coefficients are given in Fig. 20a and b while Fig. 21 shows the nett thrust coefficient.

Referring to Fig. 20a we note that the $(C_D)_A + (C_D)_B$ curves are independent of shroud length over the range tested. This is rather surprising since the shroud exit profile (Figs. 13 to 16) must vary quite rapidly with axial displacement of the exit relative to the primary shock system, and one would expect the drag curves to follow suit. The observed result is presumably valid only over a limited range because if the shroud is progressively shortened a point must eventually be reached at which the expanding primary stream restricts the secondary stream to a lesser extent. The afterbody pressures will then drop and $(C_D)_A + (C_D)_B$ will increase. Conversely, as the shroud is lengthened the flow will be governed, ultimately, by mixing processes.

$(C_D)_S$ decreases slightly as l_{13}/d_1 decreases (Fig. 20b). Since the three curves are similar in shape this reduction is probably due to the smaller skin-friction drag of the shorter shrouds. As a result (Fig. 21) the nett thrust coefficient (C_T') increases slightly with decrease in l_{13}/d_1. It is, in fact, evident that the optimum value of l_{13}/d_1 is less than unity, but as the potential gain in C_T' is obviously small the optimum shroud length was not determined precisely.

8.2.3. *The effect of δ^*/h_2 on the thrust.*—The effect of δ^*/h_2 was studied by moving one model axially within the limits of the test section and thus changing δ^* with h_2 constant. The model chosen for these tests was the C.45 nozzle and a cylindrical shroud with $a_2/a_0 = 0{\cdot}69$ and $l_{13}/d_1 = 1{\cdot}0$. No balance readings were taken, but for each axial position of the model the afterbody pressure distribution was measured over a range of jet pressure ratio. From these data we select for discussion the results at the critical jet pressure ratio (Fig. 22a and b).

In Fig. 22a the afterbody pressure distribution measured for three values of δ^*/h_2 is compared with the estimated distribution with $\delta^*/h_2 = 0$. The estimated curve assumes a normal shock in the plane of the secondary intake followed by isentropic subsonic compression. The experimental data show that the pressure recovery increases slightly with decrease in δ^*/h_2. This increase is quite small over the range tested ($0{\cdot}06 < \delta^*/h_2 < 0{\cdot}12$) but comparison with the theoretical curve indicates a marked improvement in pressure recovery as δ^*/h_2 tends to zero, and the intake shock changes from the oblique form to the normal form. The experimental data show that the critical jet pressure ratio also tends to increase slightly as δ^*/h_2 decreases; a result which is to be expected on physical grounds. Unfortunately, it was not possible to calculate a reliable value of the critical jet pressure ratio for the case when δ^*/h_2 is zero.

The afterbody plus base drag coefficient obtained by integration of the pressure distributions is plotted against δ^*/h_2 in Fig. 22b. This curve reflects the trends discussed above. Specifically, a reduction in δ^*/h_2 from 0·06 to zero decreases $(C_D)_A + (C_D)_B$ by about 0·6. Since the shroud is cylindrical and thin, and $(C_D)_S$ therefore small, this decrease in $(C_D)_A + (C_D)_B$ will increase the nett thrust coefficient (C_T') by roughly the same amount. Note, however, that this comparison is made at the critical jet pressure ratio. No data are available on the more interesting case in which the comparison is made at a fixed jet pressure ratio.

8.2.4. *The effect of a_2/a_0 and δ^*/h_2 on the thrust.*—Five shrouds of equal length but of different diameters were tested in combination with the C.45 nozzle. In this series of tests the thickness of the boundary layer at the shoulder of the afterbody was maintained constant so that both δ^*/h_2 and a_2/a_0 vary with the shroud diameter.

Curves of $(C_D)_A + (C_D)_B$ for the five models are compared with the corresponding curve for the unshrouded nozzle $(a_2/a_0 = \infty)$ in Fig. 23a. In this graph it is evident that five of the curves $(a_2/a_0 \neq 0)$ form an ordered sequence whereas the sixth $(a_2/a_0 = 0)$ is not a member of this sequence. This is presumably due to the fact that both δ^*/h_2 and a_2/a_0 vary with the shroud diameter. Provided that a_2/a_0 is greater than about 0·3, the low-energy part of the centrebody boundary layer forms but a small fraction of the air captured by the secondary intake. Under these conditions the mean total pressure of the secondary stream at the shroud entry is practically equal to the free-stream total pressure. However, as a_2/a_0 tends to zero the total pressure at the secondary intake drops to the free-stream static pressure and the form of the drag curve changes accordingly. Excluding this limiting curve it will be seen that as a_2/a_0 is reduced the critical jet pressure ratio decreases, but the corresponding minimum value of $(C_D)_A + (C_D)_B$ does not change appreciably. This type of behaviour would be expected on physical grounds.

Reducing the shroud diameter reduces the surface area of the shroud and hence the skin-friction drag. Consequently (Fig. 23b), at a given jet pressure ratio, $(C_D)_S$ decreases with decrease in a_2/a_0.

Fig. 24 shows the performance of the five shrouds with respect to the nett thrust coefficient (C_T'). Included in this figure are the corresponding curves for the unshrouded C.45 and C-D.45 reference nozzles. At a Mach number of 2·0 the operating pressure ratio of a turbojet engine lies between 10 and 20, depending on the engine design. The nett thrust developed by the C-D.45 nozzle is approximately equal to the maximum nett thrust attainable at a jet pressure ratio of 10 and is only slightly lower than this ideal value at a jet pressure ratio of 20. The curve for the C-D.45 nozzle therefore marks the upper limit of nett thrust obtainable over the operating range.

In Fig. 24 it is apparent that the performance of the shrouded nozzles is poor at low jet pressure ratios. When ${}_tp_j/p_\infty = 10$, for example, only one model $(a_2/a_0 = 0)$ gives more thrust than the unshrouded C.45 nozzle. This is because the secondary intake is running super-critical under these conditions. The pressure recovery of the secondary stream is therefore low, and the afterbody thrust is offset by the shroud drag. With increase in jet pressure ratio the comparison becomes more favourable to the shrouded models. For example, at the critical jet pressure ratio $({}_tp_j/p_\infty = 17·7)$ the nett thrust of the model with $a_2/a_0 = 0·37$ lies approximately half way between the corresponding values for the two reference models. However, even in this favourable case $(C_T)_J - (C_D)_X$ for the shrouded nozzle is some 5% less than $(C_T)_J - (C_D)_X$ for the C-D.45 nozzle. This, of course, represents a 5% increase in specific fuel consumption at the cruise condition, an increase which could scarcely be tolerated in a long-range supersonic transport.

9. *Discussion of Results. Tests with Convergent-Divergent Shrouds.*

In view of the rather disappointing performance of the cylindrical shrouds, means were sought to improve the thrust. It was argued that by decreasing a_1/a_0, and hence increasing the projected area of the afterbody, the thrust on the afterbody at the critical jet pressure ratio would be increased. However, a decrease in a_1/a_0 also increases the critical jet pressure ratio. To maintain critical operation at a fixed jet pressure ratio it therefore becomes necessary to decrease the area of the combined flows at some point within the shroud by a restriction or choke. This choke supplements the action of the expanding primary jet in restricting the flow area of the secondary stream. The most suitable form of choke would appear to be a convergent-divergent insert in a cylindrical shroud, because with this configuration the drag force acting on the convergent part of the insert is partly offset by the thrust force acting on the divergent part. The external surface of the shroud, which is cylindrical, is subject to skin-friction drag only. To improve the overall performance it is necessary to strike a favourable balance between the increase in afterbody thrust and the drag of the choke. This is a matter for experiment.

A series of tests was therefore made using the C.25 nozzle and a cylindrical shroud ($a_2/a_0 = 0{\cdot}73$, $l_{13}/d_1 = 4{\cdot}0$) with convergent-divergent inserts of different throat area (Fig. 9). The component drag coefficients are presented in Fig. 25a and b and the nett thrust coefficient in Fig. 26.

We consider first Fig. 25a which shows the effect of jet pressure ratio on $(C_D)_A + (C_D)_B$ for different values of a_4/a_3. In this graph it is apparent that when $a_4/a_3 = 1$ the critical jet pressure ratio (which lies above the test range) is considerably greater than 20. Fig. 20a shows that with the C.45 nozzle and a similar shroud ($a_2/a_0 = 0{\cdot}69$, $l_{13}/d_1 = 3{\cdot}0$) the critical jet pressure ratio is $19{\cdot}2$. Decreasing a_1/a_0 from $0{\cdot}45$ to $0{\cdot}25$ has therefore increased the critical jet pressure ratio in the expected manner. As a_4/a_3 is decreased the critical jet pressure ratio decreases (Fig. 25a) because the increased mechanical blockage assists the primary flow in restricting the passage of the secondary stream. The minimum value of $(C_D)_A + (C_D)_B$, which occurs at the critical jet pressure ratio, is independent of a_4/a_3. Comparison with Fig. 20a shows that this minimum value is $0{\cdot}15$ less than that obtained with the C.45 nozzle and a plain cylindrical shroud.

That this improvement in afterbody thrust is only obtained at the expense of a high shroud drag is shown by the curves of $(C_D)_S$ in Fig. 25b. We note that for each curve $(C_D)_S$ is a maximum at the critical jet pressure ratio, and this maximum increases as a_4/a_3 decreases. Clearly, the thrust on the divergent surface of the insert by no means annuls the drag of the convergent surface.

In Fig. 26 the nett thrust coefficient (C_T') of the models is compared with the nett thrust coefficient of the two reference models; the unshrouded C.25 and C-D.25 nozzles. The shrouded models do not compare favourably. At the higher jet pressure ratios the optimum value of a_4/a_3 is about $0{\cdot}77$ and at the critical jet pressure ratio ($_tp_j/p_\infty = 18{\cdot}4$) this model develops slightly more thrust than the C.25 nozzle. However, under these conditions $(C_T)_J - (C_D)_X$ for the shrouded model is some 9% less than $(C_T)_J - (C_D)_X$ for the C-D.25 nozzle. A loss in thrust of this order would be unacceptable in practice.

It is possible that the thrust could be increased by decreasing a_2/a_0 or l_{13}/d_1. Alternatively, some improvement might result if the internal profile of the shroud were shaped in a more subtle manner. On the other hand, it seems unlikely that either of these methods would bridge the gap between the shrouded nozzles and the C-D.25 nozzle.

10. *Conclusions.*

In the preceding text we have discussed the performance with regard to thrust of a series of aerodynamic nozzles at the design cruising speed ($M = 2$). In these models the convergent primary nozzle and conical afterbody are surrounded by a shroud. Part of the external flow (the secondary stream) is thereby trapped and compressed by the under-expanded primary jet. The resultant thrust on the conical afterbody supplements the thrust of the primary nozzle. The shrouds were either cylindrical or convergent-divergent internally, and the results are best summarised under these heads.

(1) *Convergent Primary Nozzle* ($a_1/a_0 = 0{\cdot}45$) *and Cylindrical Shrouds.*

With these models the optimum thrust was developed at the critical jet pressure ratio when the compression shock in the secondary stream intersects the leading edge of the shroud. The optimum thrust increased with decrease in shroud diameter but the variation was small provided that a_2/a_0 was less than about $0{\cdot}5$. Change in shroud length had little effect within the range $1 \leqslant l_{13}/d_1 \leqslant 3$. In comparison with the ideal thrust obtainable the performance of the aerodynamic nozzles was relatively poor. For example, the optimum thrust [expressed in terms of $(C_T)_J - (C_D)_X$] of a typical model ($a_2/a_0 = 0{\cdot}37$, $l_{13}/d_1 = 1{\cdot}0$, ${}_tp_j/p_\infty = 17{\cdot}7$) was some 5% less than that developed by the equivalent convergent-divergent reference nozzle.

(2) *Convergent Primary Nozzle* ($a_1/a_0 = 0{\cdot}25$) *and Convergent-Divergent Shrouds.*

In these tests the throat area of the primary nozzle was reduced and convergent-divergent chokes inserted in one of the cylindrical shrouds ($a_2/a_0 = 0{\cdot}73$, $l_{13}/d_1 = 4{\cdot}0$). The critical jet pressure ratio was thereby held within the required operating range ($10 < {}_tp_j/p_\infty < 20$) and, at the same time, the thrust on the afterbody was increased. Unfortunately, this increase in afterbody thrust was more than offset by the increased shroud drag. Expressed in terms of $(C_T)_J - (C_D)_X$, the thrust developed by the optimum configuration ($a_4/a_3 = 0{\cdot}77$) at the critical jet pressure ratio (${}_tp_j/p_\infty = 18{\cdot}4$) was about 9% less than the thrust developed by the equivalent convergent-divergent nozzle. The overall performance of these convergent-divergent shrouds was, therefore, slightly inferior to that obtained with the plain cylindrical shrouds.

In the experiment the range of operating conditions was limited, particularly as regards boundary-layer thickness (δ^*/h_2). Similarly, the configurations tested by no means exhaust the possibilities. For instance, no data were obtained on conical divergent shrouds. Hence it might be possible to improve on the results quoted. However, judged on the present evidence, the best of the aerodynamic nozzles tested develops 5% less thrust than the equivalent convergent-divergent nozzle at the design pressure ratio.

LIST OF SYMBOLS

The notation is shown, in part, in Fig. 4. Thrust and drag coefficients are defined in the Appendix.

Suffixes

$(\ )_0$ refers to the centrebody

$(\ )_1$ $(\ )_2$ $(\ )_3$ and $(\ )_4$ refer to the positions shown in Fig. 4

$(\ )_\infty$ denotes free-stream conditions

$(\ )_j$ refers to the primary jet

$_t(\ )$ denotes stagnation conditions

Flow parameters

M	Mach number
u	Velocity
ρ	Density
p	Static pressure

Geometrical Parameters

x	Axial distance from shroud inlet plane
r	Radial distance from axis
l	Axial length
d	Diameter
a	Cross-sectional area
h	Annular width
β	Semi-vertex angle of conical afterbody

Boundary-Layer Parameters

δ^*	Displacement thickness of boundary layer on centrebody at afterbody shoulder

Nomenclature

$_tp_j/p_\infty$ is called the jet pressure ratio

REFERENCES

No.	*Author(s)*	*Title, etc.*
1	J. Reid	The effect of a cylindrical shroud on the performance of a stationary convergent nozzle. A.R.C. R. & M. 3320. January, 1962.
2	F. D. Kochendorfer and M. D. Rousso	Performance characteristics of aircraft cooling ejectors having short cylindrical shrouds. N.A.C.A. Research Memo. E51 E01 (TIB/2767). May, 1951.
3	F. D. Kochendorfer	Note on performance of aircraft ejector nozzles at high secondary flows. N.A.C.A. Research Memo. E54 F17a (TIB/4342). August, 1954.
4	W. K. Greathouse and D. P. Hollister	Air-flow and thrust characteristics of several cylindrical cooling-air ejectors with a primary to secondary temperature ratio of 1·0. N.A.C.A. Research Memo. E52 L24 (TIB/3636). March, 1953.
5	W. K. Greathouse and W. T. Beale	Performance characteristics of several divergent-shroud aircraft ejectors. N.A.C.A. Research Memo. E55 G21a (TIB/4809). September, 1955.
6	M. A. Beheim	Off-design performance of divergent ejectors. N.A.C.A. Research Memo. E58 G10a (TIL/6188). September, 1958.
7	J. R. Mihaloew	Internal-performance evaluation of two fixed-divergent-shroud ejectors. N.A.S.A. Tech. Note D–763. January, 1961.
8	H. Pearson, J. B. Holliday and S. F. Smith	A theory of the cylindrical ejector supersonic propelling nozzle. *J. R. Ae. Soc.*, Vol. 62, No. 574. October, 1958.
9	R. R. Jessop	Tests on a two-dimensional combined intake, boundary layer bleed and ejector model at $M = 2{\cdot}41$. Vickers-Armstrong (Aircraft) Ltd. W. T. Report 2600. May, 1962.
10	J. Reid and R. C. Hastings	Experiments on the axi-symmetric flow over afterbodies and bases at $M = 2{\cdot}0$. A.R.C. 21 707. October, 1959.

APPENDIX

Definition of Thrust and Drag Coefficients

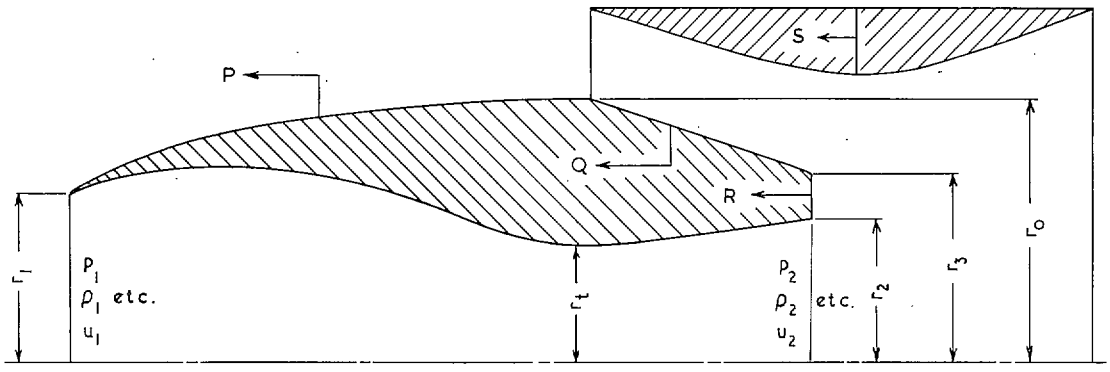

For simplicity we consider, in isolation, an axi-symmetric engine installation as shown above. It is assumed that the resultant axial force on this configuration is transmitted to the main aircraft structure by a strut. The definitions and analysis given below for this simple example may readily be adapted to cover the more practical case in which the engine installation is integrated with the wing.

In the diagram:

P, Q and R denote the axial forces on the forebody, afterbody and base, respectively

S denotes the resultant axial force on the shroud (including the fins which connect it with the engine nacelle)

a_0 is the frontal area of the nacelle, i.e. $a_0 = \pi r_0^2$

a_t is the throat area of the nozzle, i.e. $a_t = \pi r_t^2$

and $q = \frac{1}{2}\rho_\infty u_\infty^2$.

We then define the thrust and drag coefficients of the various components as follows.

(i) *Intake drag coefficient* $(C_D)_I$.

$$qa_0(C_D)_I = 2\pi \int_0^{r_1} (p_1 + \rho_1 u_1^2) r dr - \pi p_\infty r_1^2. \tag{1}$$

(ii) *Forebody drag coefficient* $(C_D)_F$.

$$qa_0(C_D)_F = \pi p_\infty (r_1^2 - r_0^2) - P. \tag{2}$$

(iii) *Afterbody drag coefficient* $(C_D)_A$.

$$qa_0(C_D)_A = \pi p_\infty (r_0^2 - r_3^2) - Q. \tag{3}$$

(iv) *Base drag coefficient* $(C_D)_B$.

$$qa_0(C_D)_B = \pi p_\infty (r_3^2 - r_2^2) - R. \tag{4}$$

(v) *Shroud drag coefficient* $(C_D)_S$.

$$qa_0(C_D)_S = -S. \tag{5}$$

(vi) *Jet thrust coefficient* $(C_T)_J$.

$$qa_0(C_T)_J = 2\pi \int_0^{r_2} (p_2 + \rho_2 u_2^2) r dr - \pi p_\infty r_2^2. \tag{6}$$

Further, let T denote the resultant axial force on the complete configuration (i.e. the force transmitted to the main aircraft structure) and define C_T by the equation

$$qa_0 C_T = T. \tag{7}$$

Then, using definitions (1) to (7) and the momentum theorem it is easily shown that:

$$C_T = (C_T)_J - [(C_D)_I + (C_D)_F + (C_D)_A + (C_D)_B + (C_D)_S]. \tag{8}$$

Writing

$$(C_D)_X = (C_D)_A + (C_D)_B + (C_D)_S \tag{9}$$

and

$$(C_D)_Y = (C_D)_I + (C_D)_F \tag{10}$$

equation (8) becomes

$$C_T = [(C_T)_J - (C_D)_X] - (C_D)_Y. \tag{11}$$

Now, in the present experiment, the geometry of the afterbody, base, nozzle and shroud varies, but a_t/a_0 is constant for each series of tests. For comparative purposes we may therefore assume that $(C_D)_I$ and $(C_D)_F$, and hence $(C_D)_Y$, are also constant at a given value of ${}_tp_j/p_\infty$. On this basis equation (11) shows that $(C_T)_J - (C_D)_X$ is a direct measure of C_T (the propulsive force transmitted to the aircraft structure).

We might, therefore, reasonably plot the experimental thrust data in terms of $(C_T)_J - (C_D)_X$, but if this is done we find that the curves lie rather close together and are difficult to distinguish. Accordingly a reference datum $(C_T)_J{}^*$ is defined as follows:

$(C_T)_J{}^*$ is the measured jet thrust coefficient of a convergent nozzle with the same value of a_t/a_0 as the nozzle in the test model.

We then define the nett thrust coefficient $(C_T{}')$ by the equation:

$$C_T{}' = (C_T)_J - (C_T)_J{}^* - (C_D)_X \tag{12}$$

and present the results in terms of $C_T{}'$. In this way an open scale is obtained and small differences in the thrust performance are readily detected.

It is evident that if the nozzle in the test model is itself convergent

$$(C_T)_J = (C_T)_J{}^* \text{ (by definition)}$$

so that

$$C_T{}' = -(C_D)_X. \tag{13}$$

[Note that the definitions of $(C_D)_F$, $(C_D)_A$ and $(C_D)_S$ include forces due to both pressure and skin friction. These are, in fact, 'total' drag coefficients.]

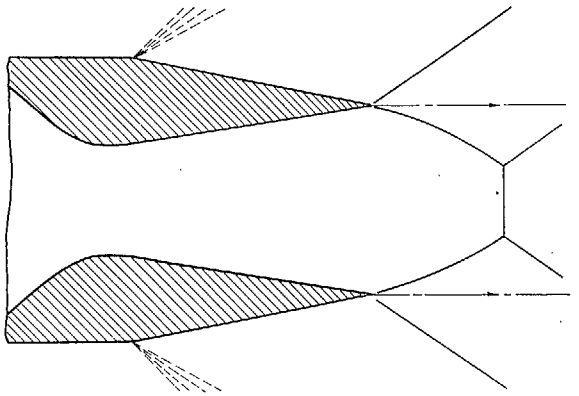

(a) NOZZLE RUNNING AT DESIGN PRESSURE RATIO.

DENOTES A REGION OF SEPARATED FLOW.

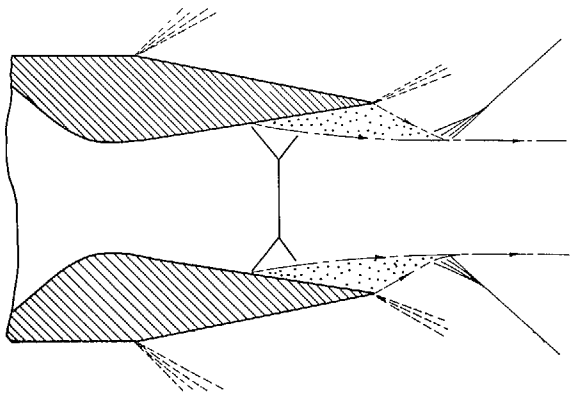

(b) NOZZLE RUNNING OVER-EXPANDED.

FIGS. 1a and b. The effect of jet pressure ratio on the flow pattern in a convergent-divergent nozzle.

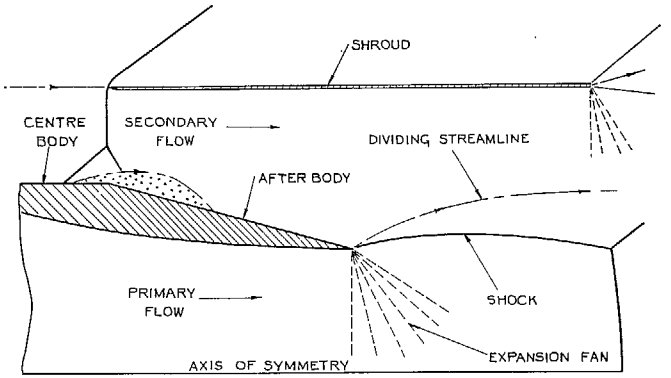

(a) AXI-SYMMETRIC AERODYNAMIC NOZZLE.

DENOTES A REGION OF SEPARATED FLOW.

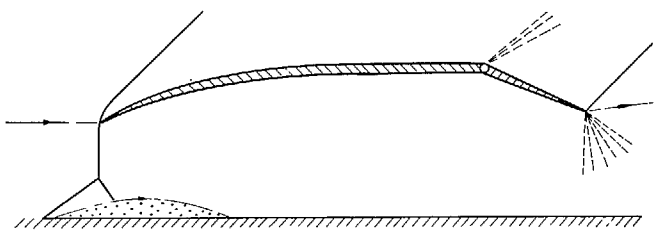

(b) SIDE INTAKE CONTROLLED BY HINGED EXIT FLAP.

FIGS. 2a and b. The principle of the aerodynamic nozzle.

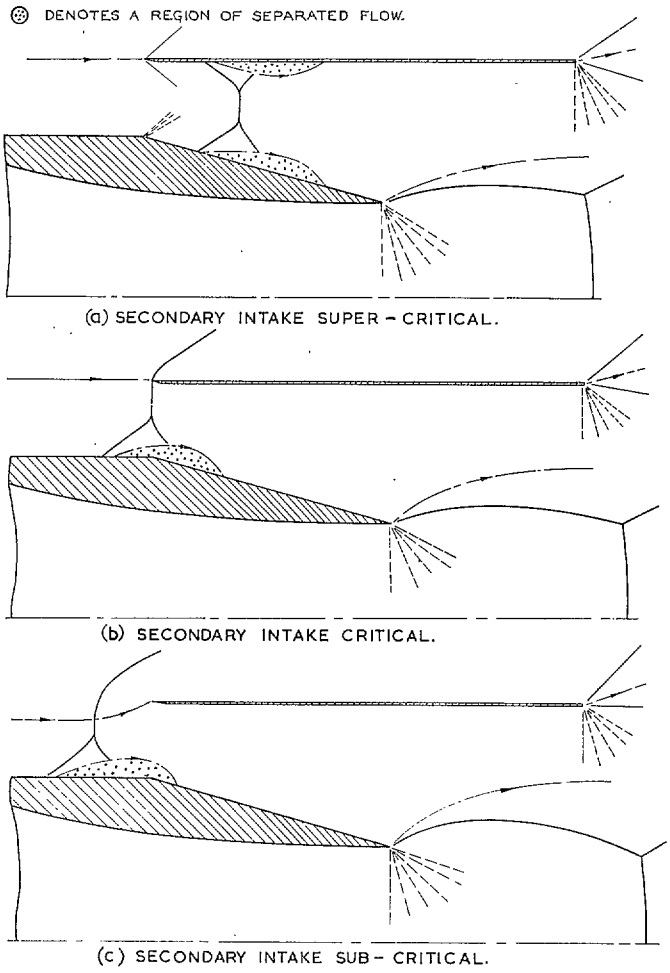

FIGS. 3a to c. Flow regimes in the aerodynamic nozzle.

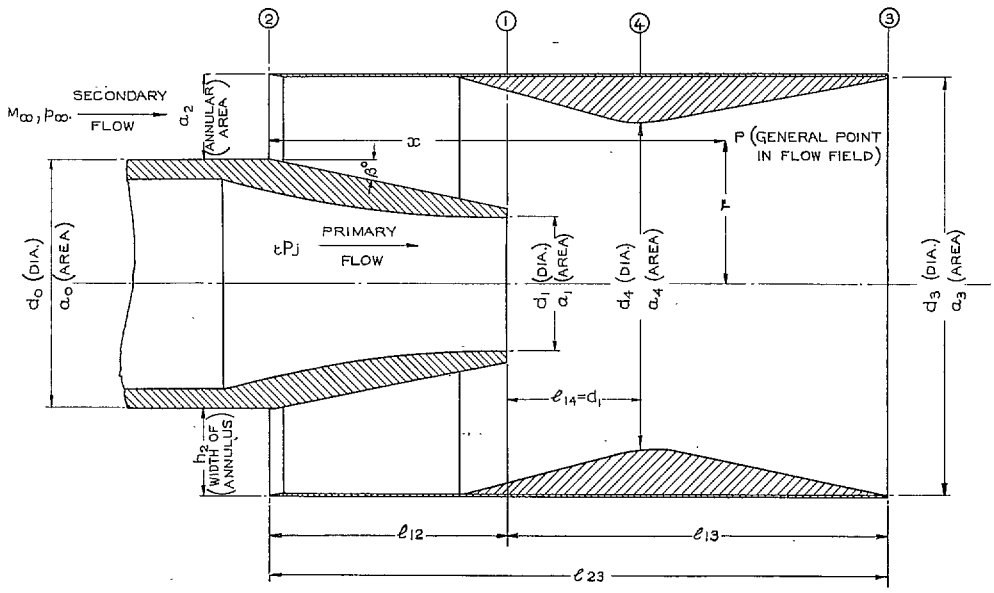

FIG. 4. Schematic diagram showing notation.

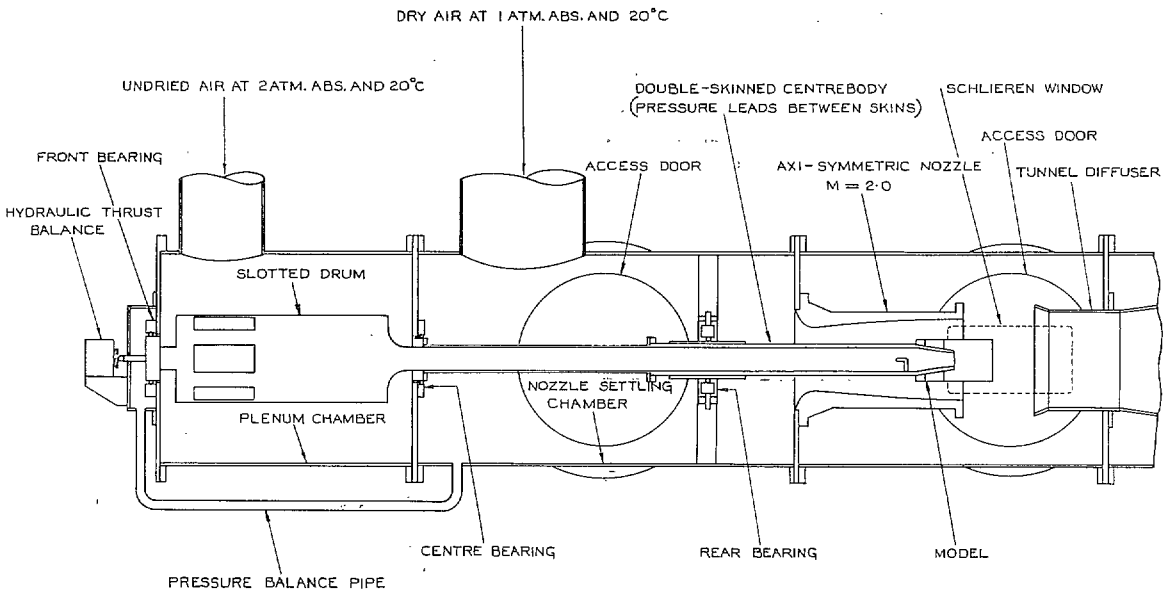

FIG. 5. The Jet Interference Tunnel (No. 16).

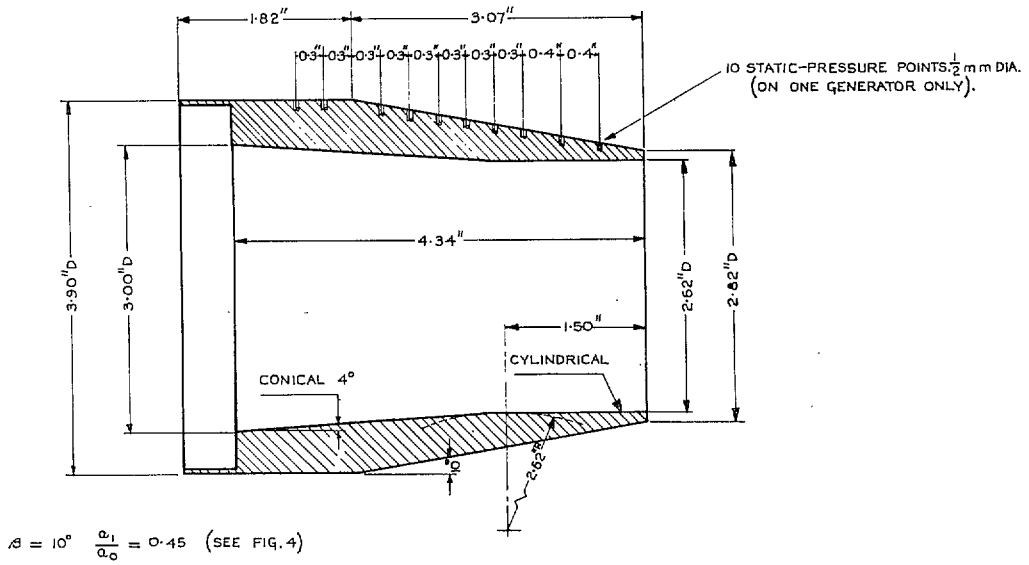

FIG. 6. Convergent nozzle used with cylindrical shrouds. Code No. C.45.

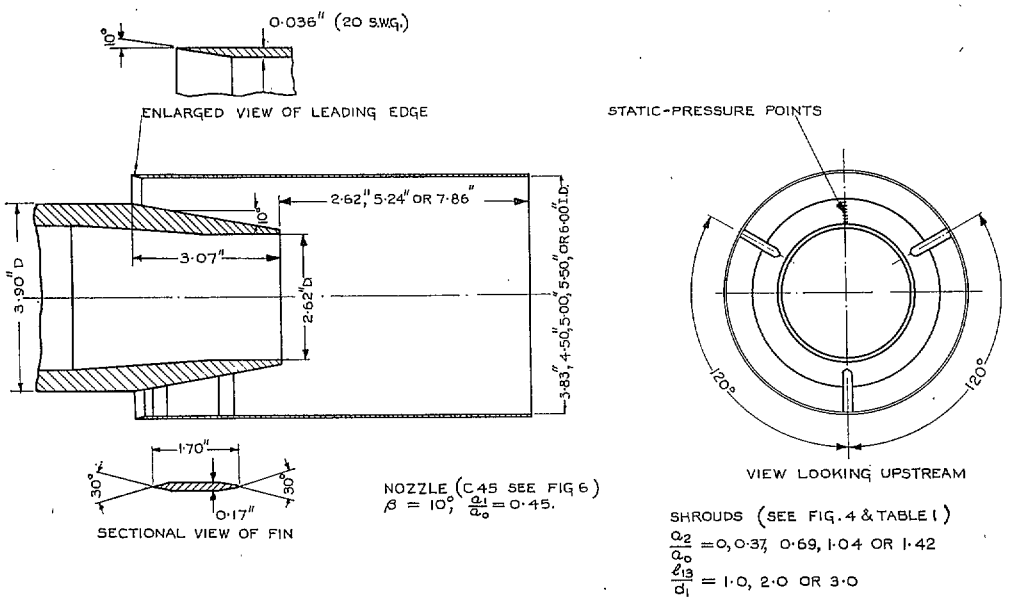

FIG. 7. Convergent nozzle with cylindrical shrouds.

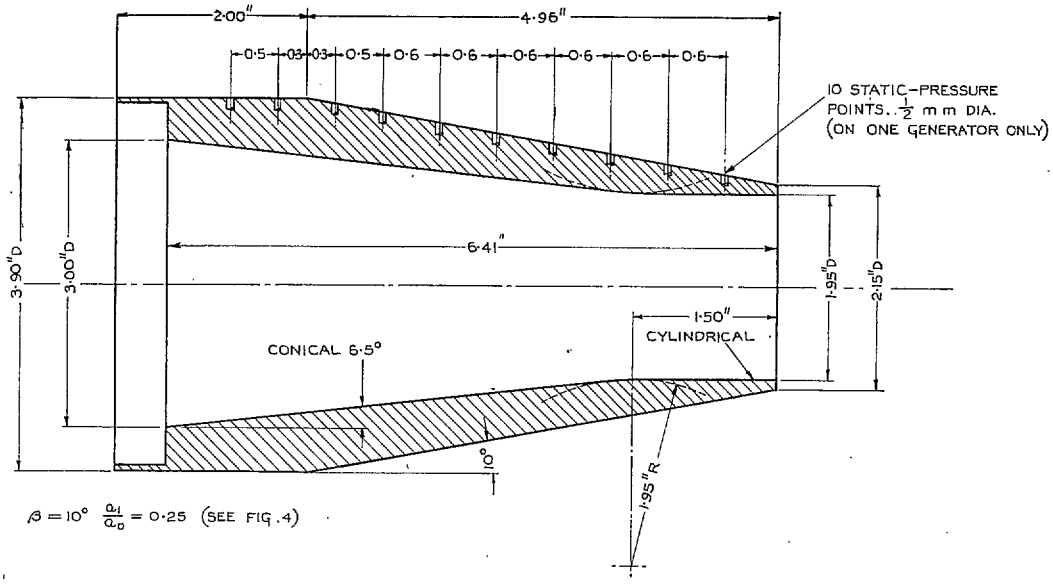

FIG. 8. Convergent nozzle used with convergent-divergent shrouds. Code No. C.25.

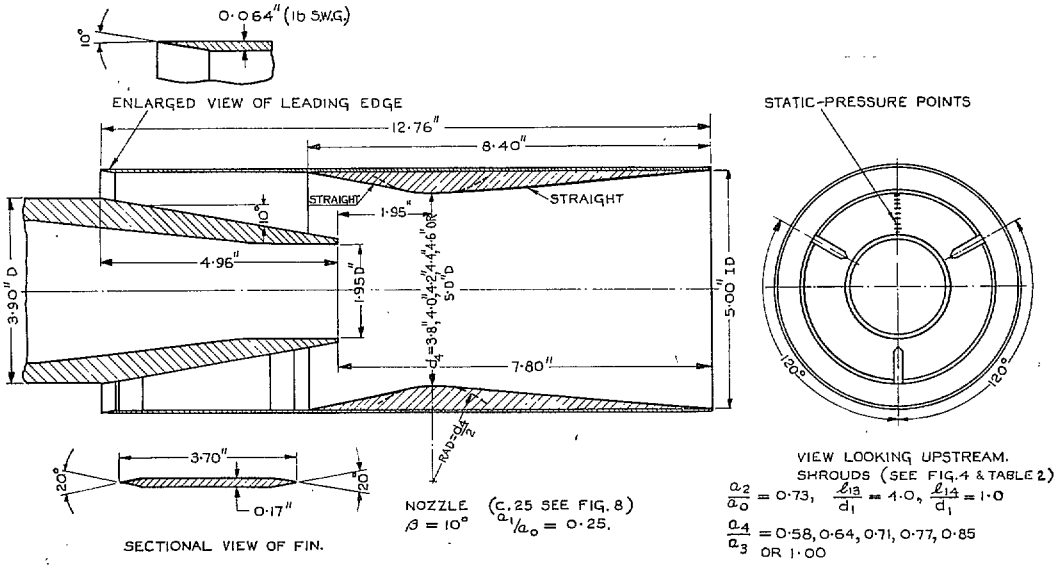

FIG. 9. Convergent nozzle with convergent-divergent shrouds.

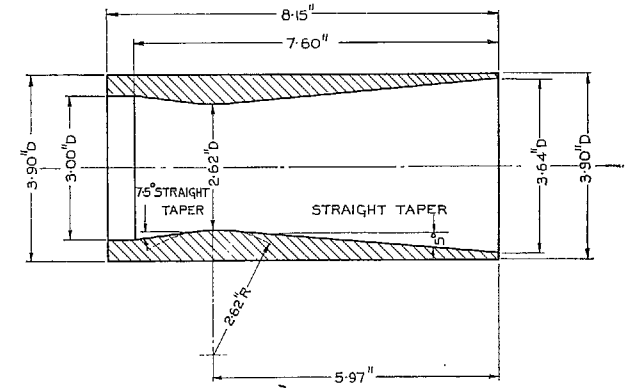

NOZZLE DIVERGENCE ANGLE = 5°
NOZZLE DESIGN PRESSURE RATIO = 10·0
NOZZLE DESIGN MACH NUMBER = 2·16

(a) $\frac{\text{THROAT AREA}}{\text{MAX. BODY AREA}} = 0{\cdot}45$ CODE No. C–D 45.

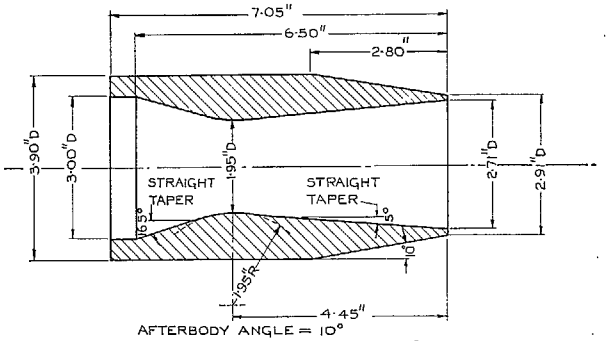

AFTERBODY ANGLE = 10°
NOZZLE DIVERGENCE ANGLE = 5°
NOZZLE DESIGN PRESSURE RATIO = 10·0
NOZZLE DESIGN MACH NUMBER = 2·16

(b) $\frac{\text{THROAT AREA}}{\text{MAX. BODY AREA}} = 0{\cdot}25$ CODE No. C–D 25.

FIGS. 10a and b. Convergent-divergent reference nozzles.

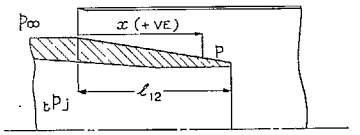

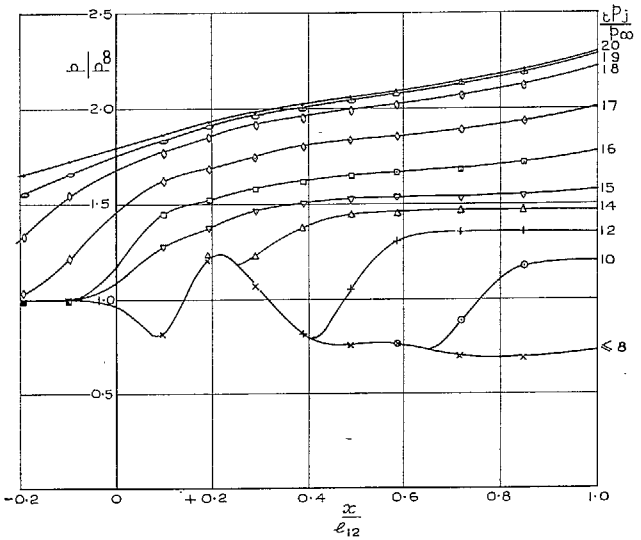

CONVERGENT NOZZLE. C.45.

CYLINDRICAL SHROUD. $M_\infty = 2{\cdot}0$, $\frac{\delta^*}{h_2} = 0{\cdot}12$, $\frac{a_2}{a_0} = 0{\cdot}69$, $\frac{\ell_{13}}{d_1} = 1{\cdot}0$.

FIG. 11. The effect of jet pressure ratio on the afterbody pressure distribution.

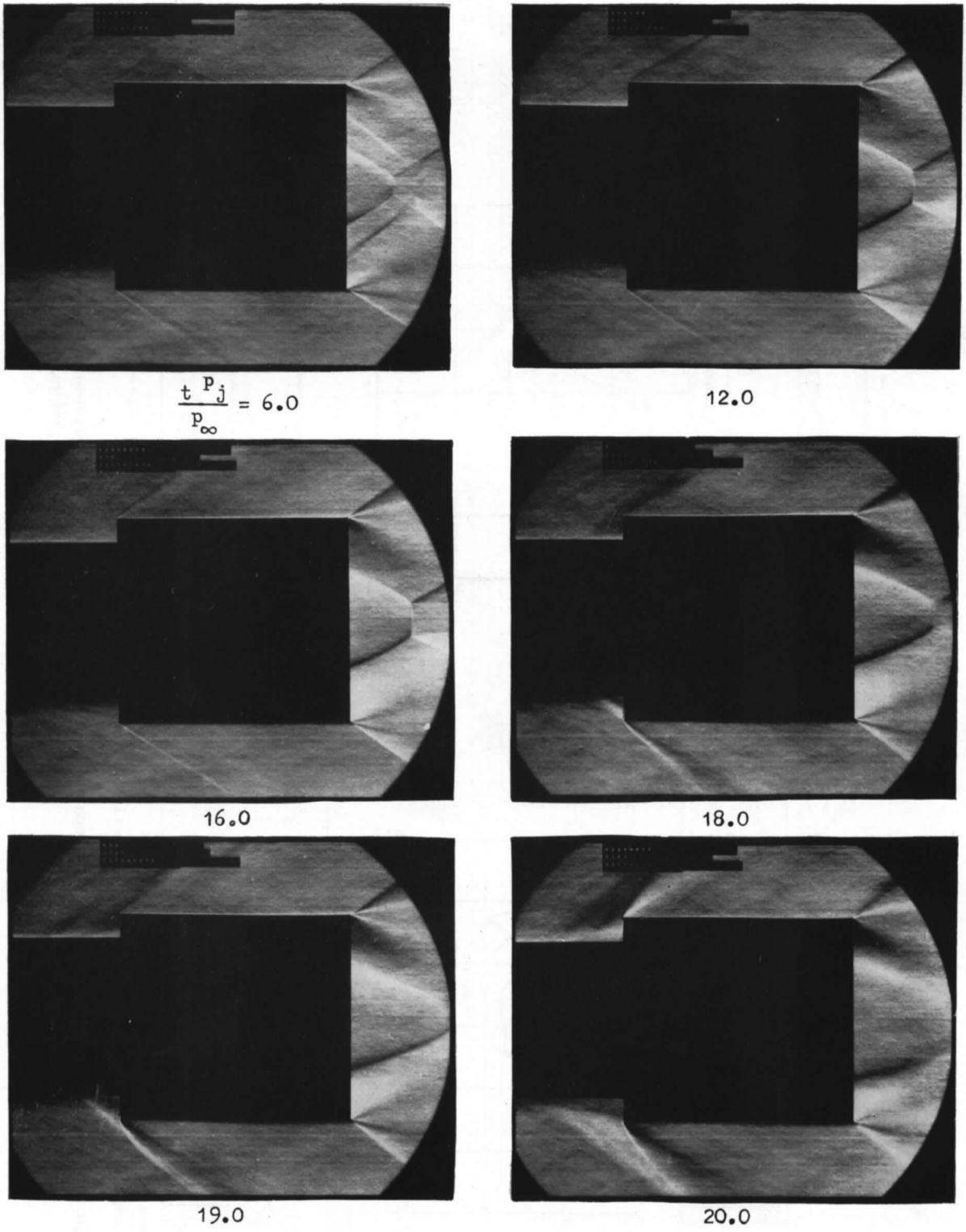

Convergent nozzle. C.45

Cylindrical shroud. $M_\infty = 2.0$, $\frac{\delta^*}{h_2} \simeq 0.12$, $\frac{a_2}{a_o} = 0.69$, $\frac{\ell_{13}}{d_1} = 1.0$

FIG. 12. Schlieren photographs showing the effect of jet pressure ratio on the flow.

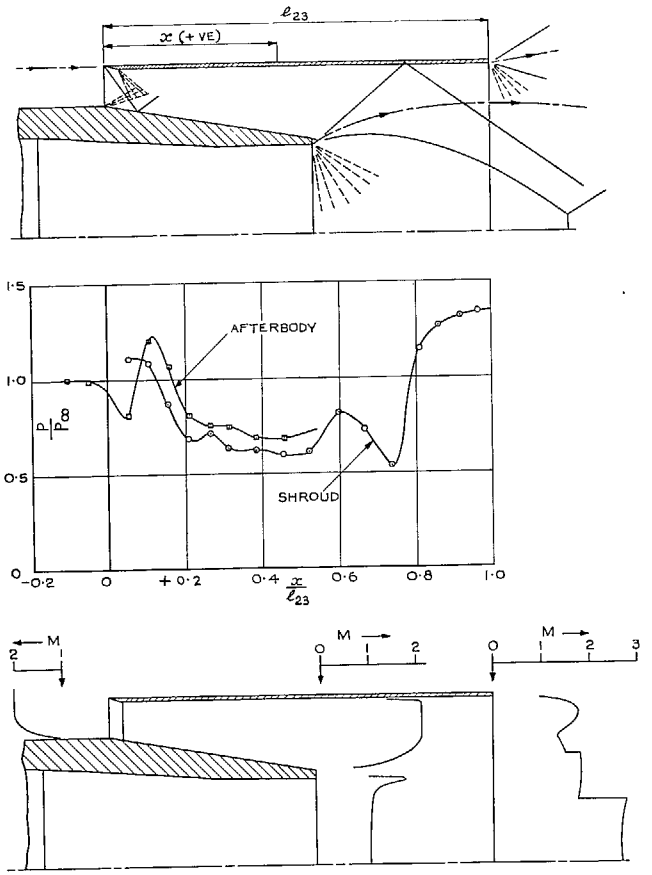

CONVERGENT NOZZLE. C.45.
CYLINDRICAL SHROUD. $M_\infty = 2{\cdot}0$, $\frac{\delta^*}{h_2} = 0{\cdot}12$, $\frac{a_2}{a_0} = 0{\cdot}69$, $\frac{\ell_{13}}{d_1} = 1{\cdot}0$.

FIG. 13. Surface pressure distribution and Mach number profiles. ${}_{\iota}p_j/p_\infty = 6{\cdot}0$.

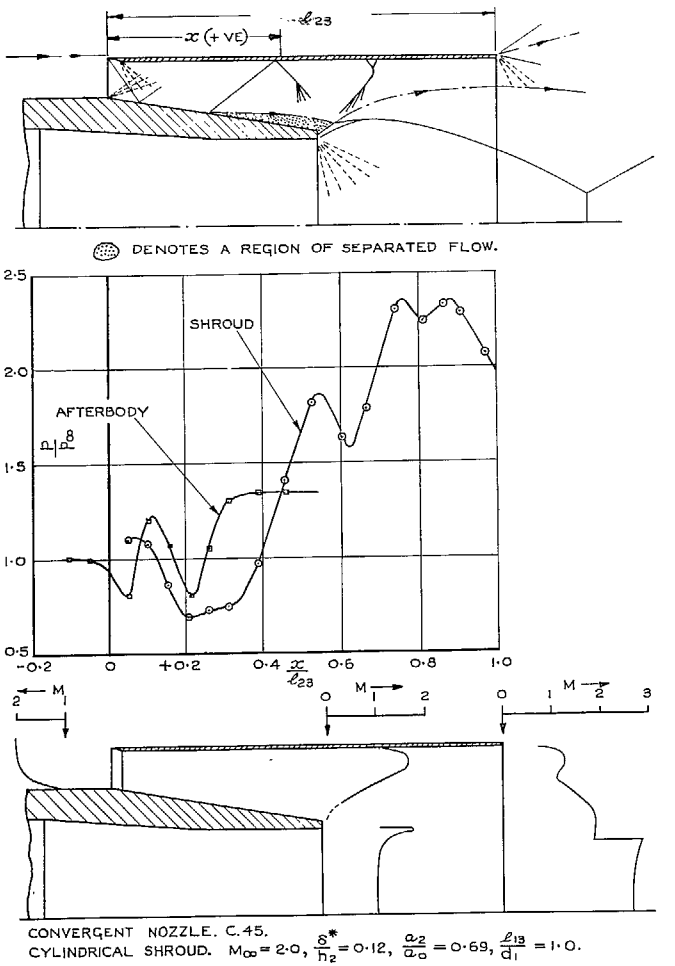

CONVERGENT NOZZLE. C.45.
CYLINDRICAL SHROUD. $M_\infty = 2{\cdot}0$, $\frac{\delta^*}{h_2} = 0{\cdot}12$, $\frac{a_2}{a_0} = 0{\cdot}69$, $\frac{\ell_{13}}{d_1} = 1{\cdot}0$.

FIG. 14. Surface pressure distribution and Mach number profiles. ${}_{\iota}p_j/p_\infty = 12{\cdot}0$.

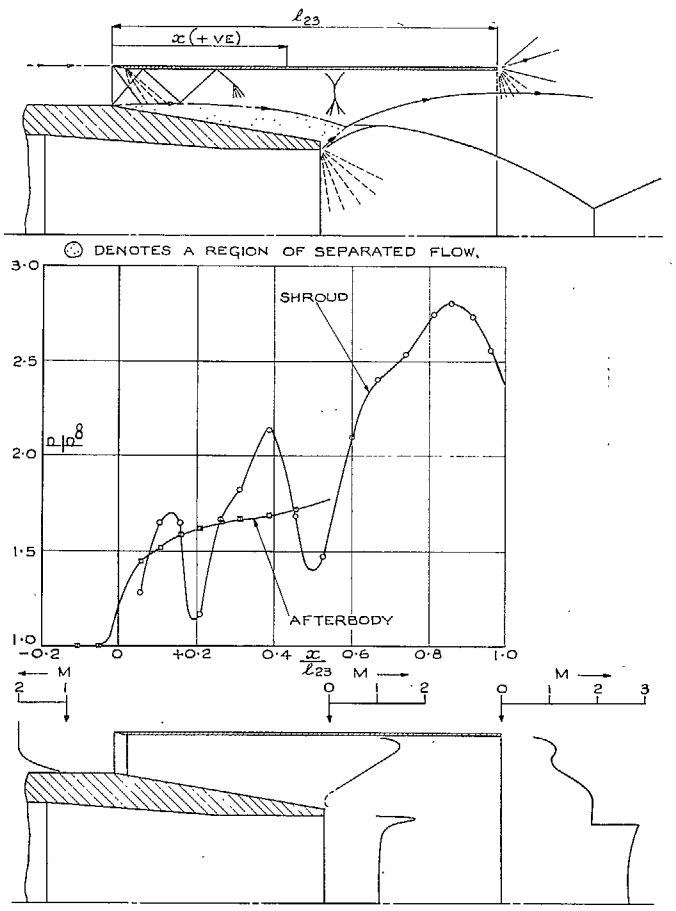

CONVERGENT NOZZLE. C. 45.
CYLINDRICAL SHROUD. $M_\infty = 2{\cdot}0$, $\frac{\delta^*}{h_2} = 0{\cdot}12$, $\frac{a_2}{a_0} = 0{\cdot}69$, $\frac{\ell_{13}}{d_1} = 1{\cdot}0$.

FIG. 15. Surface pressure distribution and Mach number profiles. ${}_tp_j/p_\infty = 16{\cdot}0$.

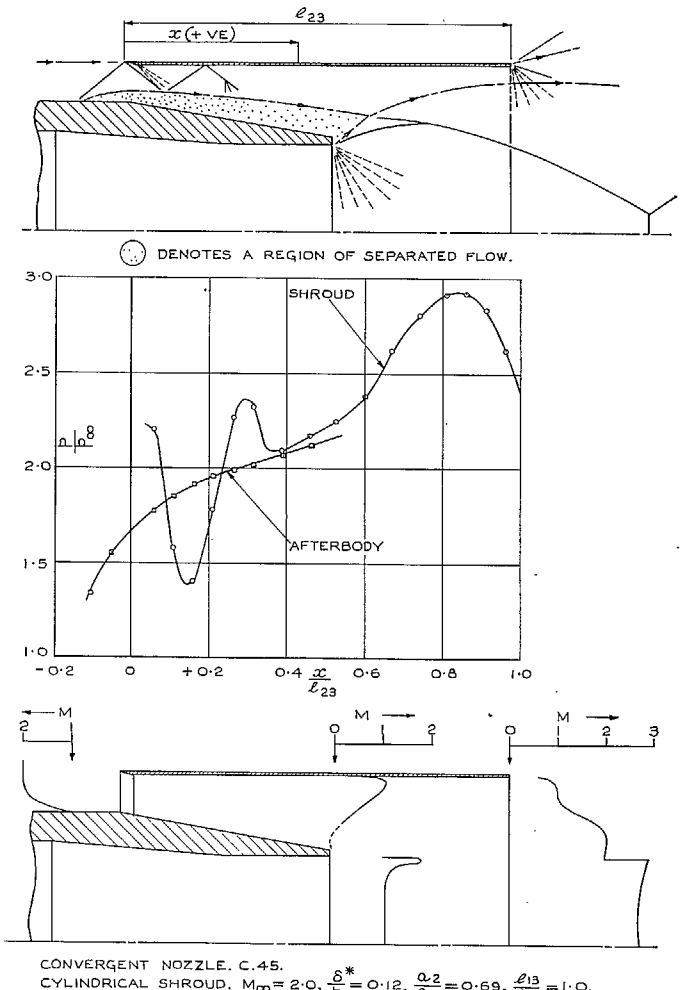

CONVERGENT NOZZLE. C.45.
CYLINDRICAL SHROUD. $M_\infty = 2{\cdot}0$, $\frac{\delta^*}{h_2} = 0{\cdot}12$, $\frac{a_2}{a_0} = 0{\cdot}69$, $\frac{\ell_{13}}{d_1} = 1{\cdot}0$.

FIG. 16. Surface pressure distribution and Mach number profiles. ${}_tp_j/p_\infty = 18{\cdot}0$.

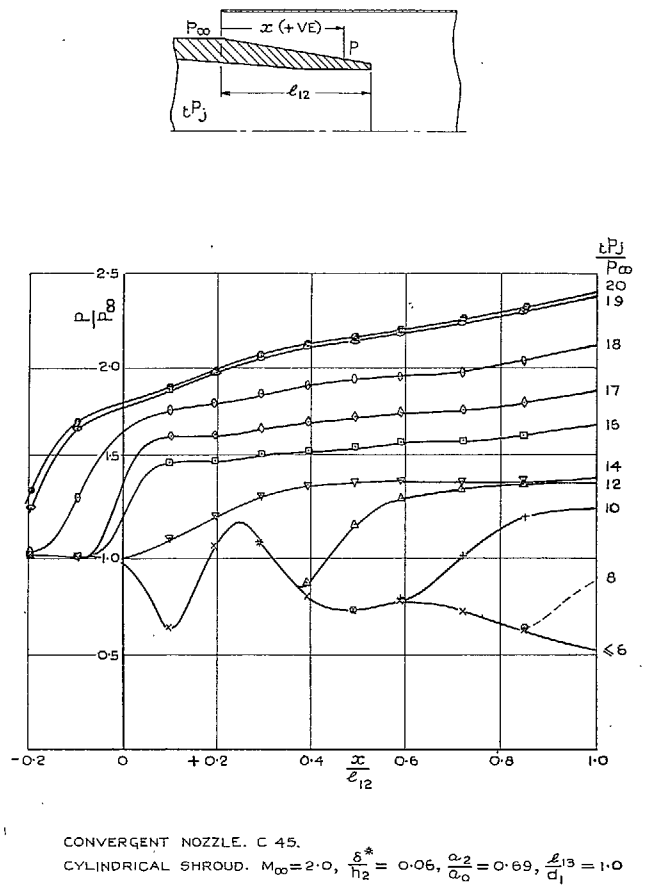

CONVERGENT NOZZLE. C 45.
CYLINDRICAL SHROUD. $M_\infty = 2{\cdot}0$, $\frac{\delta^*}{h_2} = 0{\cdot}06$, $\frac{a_2}{a_0} = 0{\cdot}69$, $\frac{\ell_{13}}{d_1} = 1{\cdot}0$

FIG. 17. The effect of jet pressure ratio on the afterbody pressure distribution.

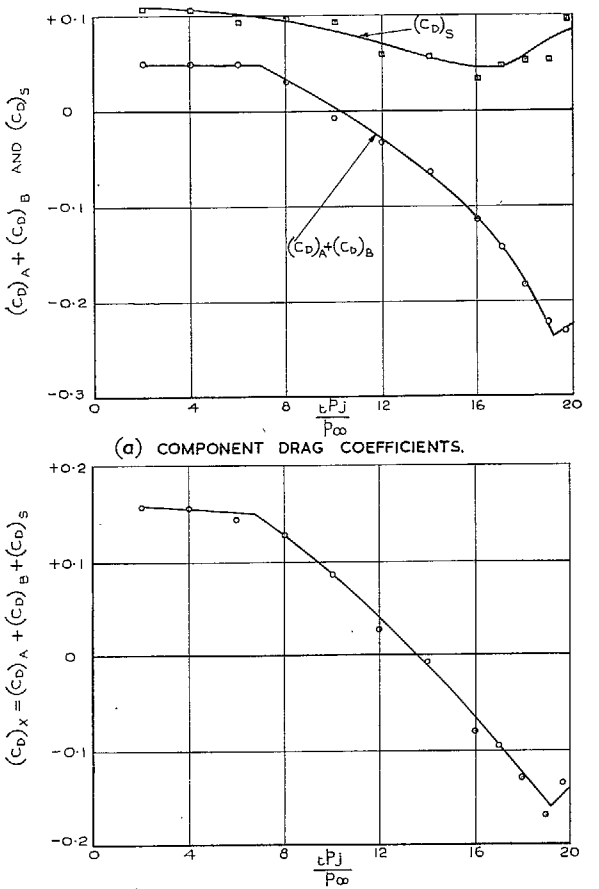

CONVERGENT NOZZLE. C. 45.
CYLINDRICAL SHROUD. $M_\infty = 2{\cdot}0$, $\frac{\delta^*}{h_2} = 0{\cdot}06$, $\frac{a_2}{a_0} = 0{\cdot}69$, $\frac{\ell_{13}}{d_1} = 1{\cdot}0$.

FIGS. 18a and b. The effect of jet pressure ratio on the component and total drag coefficients.

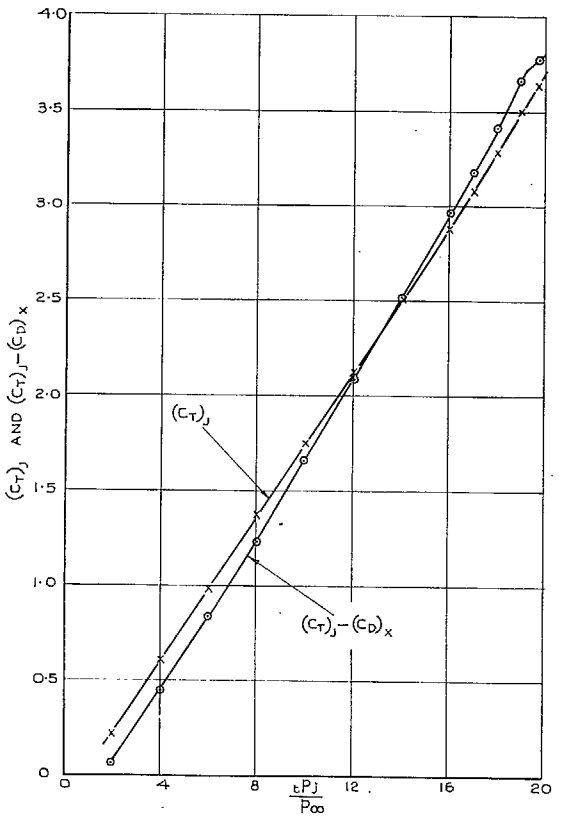

CONVERGENT NOZZLE. C.45
CYLINDRICAL SHROUD. $M_\infty = 2{\cdot}0$, $\frac{\delta^*}{h_2} = 0{\cdot}06$, $\frac{a_2}{a_0} = 0{\cdot}69$, $\frac{l_{13}}{d_1} = 1{\cdot}0$.

FIG. 19. The effect of jet pressure ratio on the thrust coefficients.

l_{13}/d_1	1·0	2·0	3·0
SYMBOL	□	○	◇

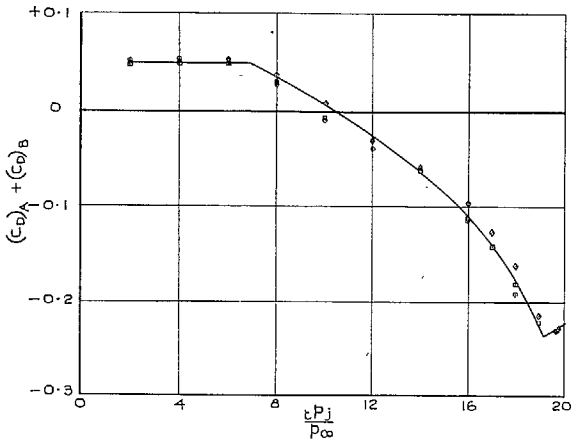

(a) AFTERBODY PLUS BASE DRAG COEFFICIENT.

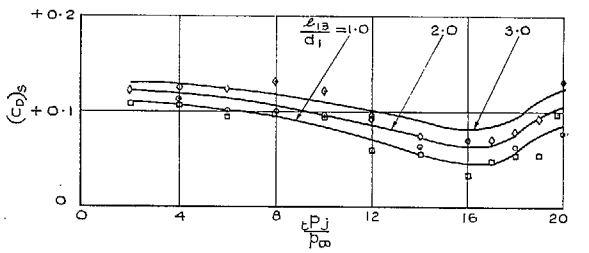

(b) SHROUD DRAG COEFFICIENT.

CONVERGENT NOZZLE. C.45.
CYLINDRICAL SHROUDS. $M_\infty = 2{\cdot}0$, $\frac{\delta^*}{h_2} = 0{\cdot}06$, $\frac{a_2}{a_0} = 0{\cdot}69$.

FIGS. 20a and b. The effect of ${}_tp_j/p_\infty$ and l_{13}/d_1 on the component drag coefficients.

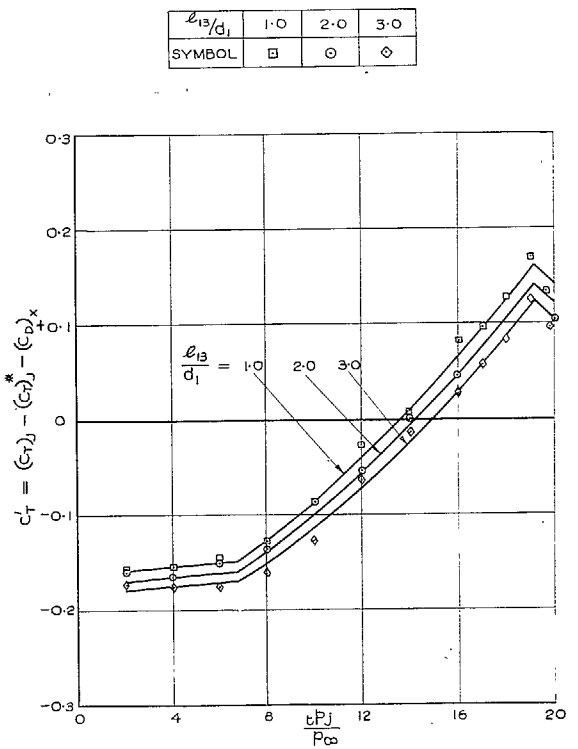

FIG. 21. The effect of ${}_tp_j/p_\infty$ and l_{13}/d_1 on the nett thrust coefficient.

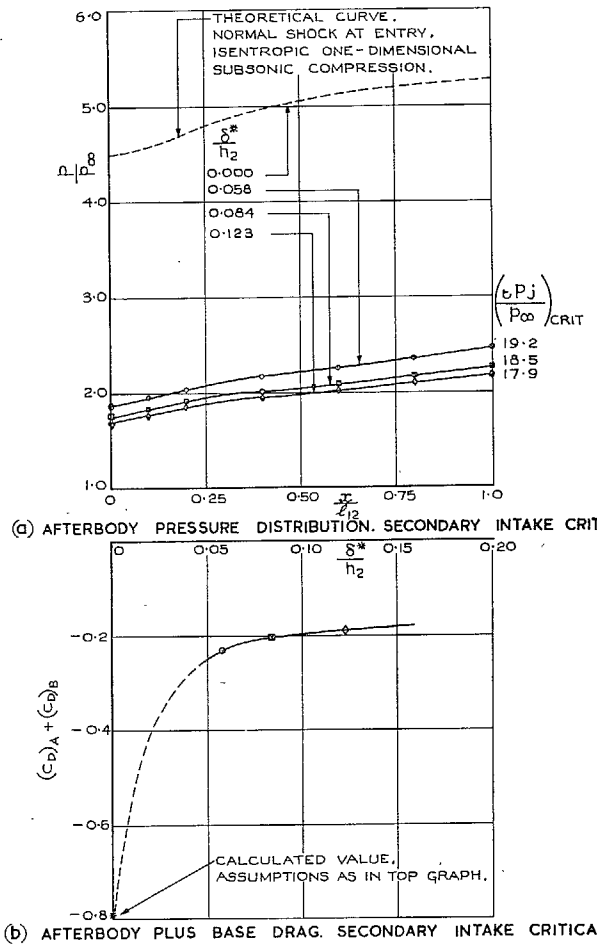

FIGS. 22a and b. The effect of δ^*/h_2 on the afterbody pressure distribution and $(C_D)_A + (C_D)_B$ with the secondary intake critical.

SYMBOL	×	⊙	+	⊡	◇	△
a_2/a_0	0·00	0·37	0·69	1·04	1·42	∞
δ^*/h_2	—	0·10	0·06	0·04	0·03	0·00

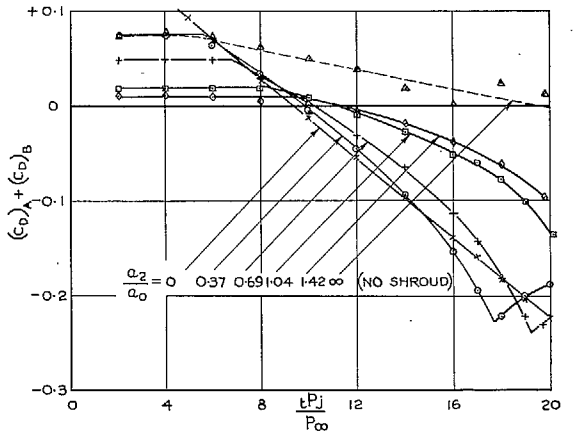

(a) AFTERBODY PLUS BASE DRAG COEFFICIENT.

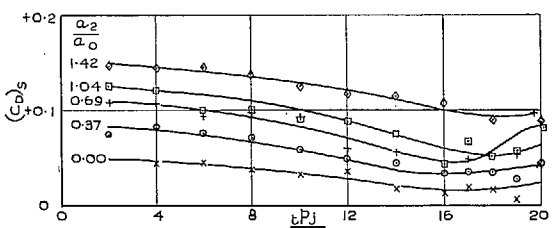

(b) SHROUD DRAG COEFFICIENT.

CONVERGENT NOZZLE C.45.
CYLINDRICAL SHROUDS. $M_\infty = 2{\cdot}0$, $\frac{\ell_{13}}{d_1} = 1{\cdot}0$.

FIGS. 23a and b. The effect of ${}_tp_j/p_\infty$, a_2/a_0 and δ^*/h_2 on the component drag coefficients.

SYMBOL	×	⊙	+	⊡	◇
a_2/a_0	0·00	0·37	0·69	1·04	1·42
δ^*/h_2	—	0·10	0·06	0·04	0·03

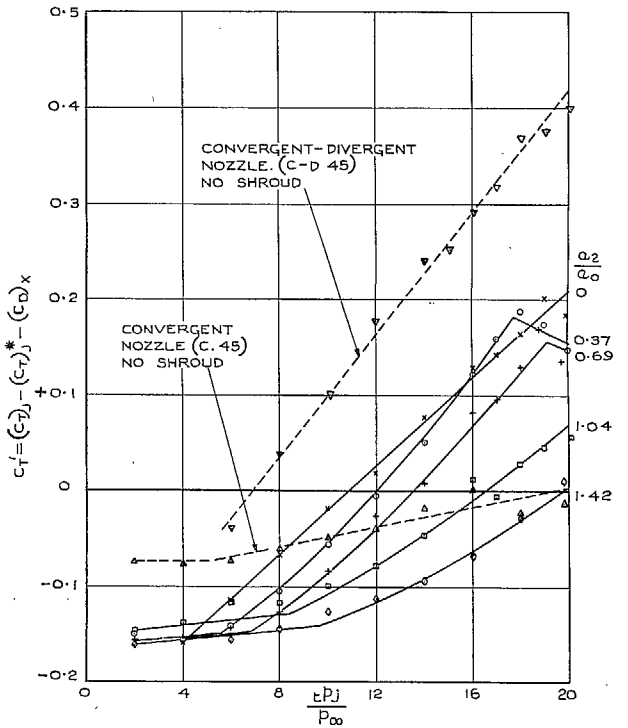

FULL LINES DENOTE CONVERGENT NOZZLE (C. 45) WITH CYLINDRICAL SHROUDS. $M_\infty = 2{\cdot}0$, $\frac{\ell_{13}}{d_1} = 1{\cdot}0$.

FIG. 24. The effect of ${}_tp_j/p_\infty$, a_2/a_0 and δ^*/h_2 on the nett thrust coefficient.

(90186) Wt. 66/2301 K.5 10/64 Hw.

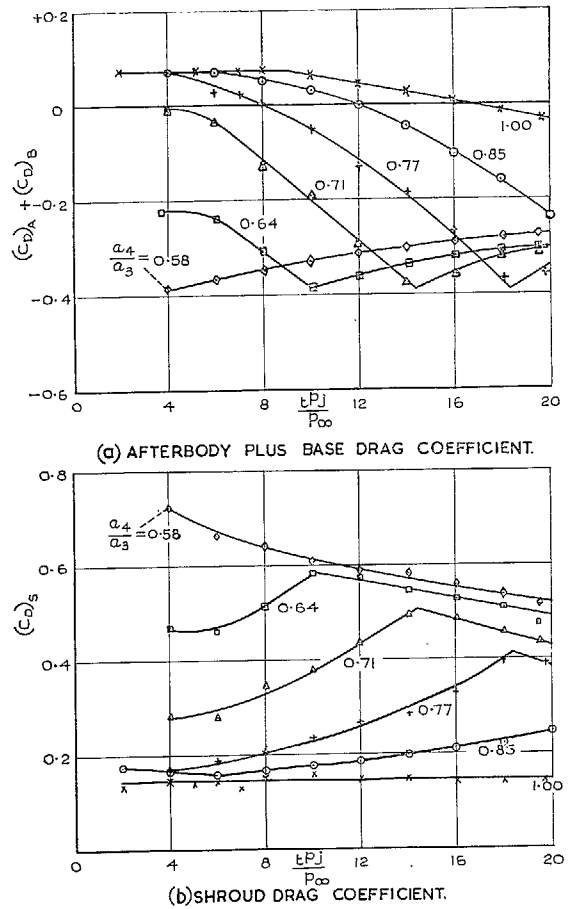

CONVERGENT NOZZLE. C. 25.
CONVERGENT-DIVERGENT SHROUDS. $M_\infty = 2·0$, $\frac{\delta^*}{h_2} = 0·06$, $\frac{a_2}{a_0} = 0·73$, $\frac{\ell_{13}}{d_1} = 4·0$.

FIGS. 25a and b. The effect of ${}_tp_j/p_\infty$ and a_4/a_3 on the component drag coefficients.

SYMBOL	×	⊙	+	△	⊡	◇
a_4/a_3	1·00	0·85	0·77	0·71	0·64	0·58

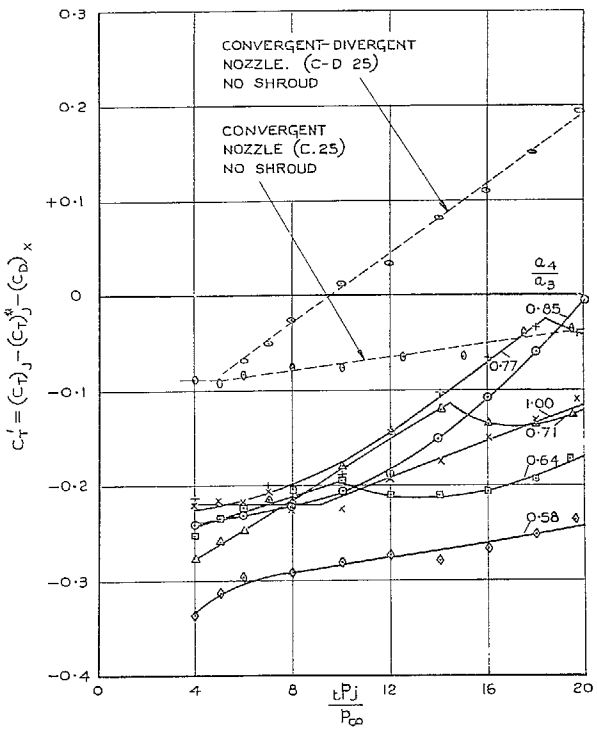

FULL LINES DENOTE CONVERGENT NOZZLE (C. 25) WITH CONVERGENT-DIVERGENT SHROUDS. $M_\infty = 2·0$, $\frac{\delta^*}{h_2} = 0·06$, $\frac{a_2}{a_0} = 0·73$, $\frac{\ell_{13}}{d_1} = 4·0$.

FIG. 26. The effect of ${}_tp_j/p_\infty$ and a_4/a_3 on the nett thrust coefficient.

Publications of the Aeronautical Research Council

ANNUAL TECHNICAL REPORTS OF THE AERONAUTICAL RESEARCH COUNCIL (BOUND VOLUMES)

1942 Vol. I. Aero and Hydrodynamics, Aerofoils, Airscrews, Engines. 75*s.* (post 2*s.* 9*d.*)
Vol. II. Noise, Parachutes, Stability and Control, Structures, Vibration, Wind Tunnels. 47*s.* 6*d.* (post 2*s.* 3*d.*)

1943 Vol. I. Aerodynamics, Aerofoils, Airscrews. 80*s.* (post 2*s.* 6*d.*)
Vol. II. Engines, Flutter, Materials, Parachutes, Performance, Stability and Control, Structures. 90*s.* (post 2*s.* 9*d.*)

1944 Vol. I. Aero and Hydrodynamics, Aerofoils, Aircraft, Airscrews, Controls. 84*s.* (post 3*s.*)
Vol. II. Flutter and Vibration, Materials, Miscellaneous, Navigation, Parachutes, Performance, Plates and Panels, Stability, Structures, Test Equipment, Wind Tunnels. 84*s.* (post 3*s.*)

1945 Vol. I. Aero and Hydrodynamics, Aerofoils. 130*s.* (post 3*s.* 6*d.*)
Vol. II. Aircraft, Airscrews, Controls. 130*s.* (post 3*s.* 6*d.*)
Vol. III. Flutter and Vibration, Instruments, Miscellaneous, Parachutes, Plates and Panels, Propulsion. 130*s.* (post 3*s.* 3*d.*)
Vol. IV. Stability, Structures, Wind Tunnels, Wind Tunnel Technique. 130*s.* (post 3*s.* 3*d.*)

1946 Vol. I. Accidents, Aerodynamics, Aerofoils and Hydrofoils. 168*s.* (post 3*s.* 9*d.*)
Vol. II. Airscrews, Cabin Cooling, Chemical Hazards, Controls, Flames, Flutter, Helicopters, Instruments and Instrumentation, Interference, Jets, Miscellaneous, Parachutes. 168*s.* (post 3*s.* 3*d.*)
Vol. III. Performance, Propulsion, Seaplanes, Stability, Structures, Wind Tunnels. 168*s.* (post 3*s.* 6*d.*)

1947 Vol. I. Aerodynamics, Aerofoils, Aircraft. 168*s.* (post 3*s.* 9*d.*)
Vol. II. Airscrews and Rotors, Controls, Flutter, Materials, Miscellaneous, Parachutes, Propulsion, Seaplanes, Stability, Structures, Take-off and Landing. 168*s.* (post 3*s.* 9*d.*)

1948 Vol. I. Aerodynamics, Aerofoils, Aircraft, Airscrews, Controls, Flutter and Vibration, Helicopters, Instruments, Propulsion, Seaplane, Stability, Structures, Wind Tunnels. 130*s.* (post 3*s.* 3*d.*)
Vol. II. Aerodynamics, Aerofoils, Aircraft, Airscrews, Controls, Flutter and Vibration, Helicopters, Instruments, Propulsion, Seaplane, Stability, Structures, Wind Tunnels. 110*s.* (post 3*s.* 3*d.*)

Special Volumes

Vol. I. Aero and Hydrodynamics, Aerofoils, Controls, Flutter, Kites, Parachutes, Performance, Propulsion, Stability. 126*s.* (post 3*s.*)
Vol. II. Aero and Hydrodynamics, Aerofoils, Airscrews, Controls, Flutter, Materials, Miscellaneous, Parachutes, Propulsion, Stability, Structures. 147*s.* (post 3*s.*)
Vol. III. Aero and Hydrodynamics, Aerofoils, Airscrews, Controls, Flutter, Kites, Miscellaneous, Parachutes, Propulsion, Seaplanes, Stability, Structures, Test Equipment. 189*s.* (post 3*s.* 9*d.*)

Reviews of the Aeronautical Research Council

1939–48 3*s.* (post 6*d.*) 1949–54 5*s.* (post 5*d.*)

Index to all Reports and Memoranda published in the Annual Technical Reports

1909–1947 R. & M. 2600 (out of print)

Indexes to the Reports and Memoranda of the Aeronautical Research Council

Between Nos. 2351–2449	R. & M. No. 2450 2*s.* (post 3*d.*)
Between Nos. 2451–2549	R. & M. No. 2550 2*s.* 6*d.* (post 3*d.*)
Between Nos. 2551–2649	R. & M. No. 2650 2*s.* 6*d.* (post 3*d.*)
Between Nos. 2651–2749	R. & M. No. 2750 2*s.* 6*d.* (post 3*d.*)
Between Nos. 2751–2849	R. & M. No. 2850 2*s.* 6*d.* (post 3*d.*)
Between Nos. 2851–2949	R. & M. No. 2950 3*s.* (post 3*d.*)
Between Nos. 2951–3049	R. & M. No. 3050 3*s.* 6*d.* (post 3*d.*)
Between Nos. 3051–3149	R. & M. No. 3150 3*s.* 6*d.* (post 3*d.*)

HER MAJESTY'S STATIONERY OFFICE

from the addresses overleaf

Printed and published by
HER MAJESTY'S STATIONERY OFFICE

To be purchased from
York House, Kingsway, London W.C.2
423 Oxford Street, London W.1
13A Castle Street, Edinburgh 2
109 St. Mary Street, Cardiff
39 King Street, Manchester 2
50 Fairfax Street, Bristol 1
35 Smallbrook, Ringway, Birmingham 5
80 Chichester Street, Belfast 1
or through any bookseller

Printed in England

S.O. Code No. 23-3382